Acta Crystallographica Section A
Foundations of Crystallography
ISSN 0108-7673

Received 17 March 2004
Accepted 28 July 2004

Effects of near-neighbor correlations on the diffuse scattering from a one-dimensional paracrystal

Frédéric Leroy,[a] Rémi Lazzari[b]* and Gilles Renaud[a]

[a]CEA-Grenoble, Département de Recherche Fondamentale sur la Matière Condensée, Service de Physique des Matériaux et Microstructures, Nanostructures et Rayonnement Synchrotron, 17 Avenue des Martyrs, F-38054 Grenoble CEDEX 9, France, and [b]Groupe de Physique des Solides, CNRS UMR 7588 – Universités Paris 6 et 7, Campus Boucicaut, 140 Rue de Lourmel, 75015 Paris, France. Correspondence e-mail: lazzari@gps.jussieu.fr

The one-dimensional paracrystal model is generalized by folding the lattice sites with objects whose scattering lengths or sizes and separation display a spatial correlation from cell to cell. A general theory to calculate the diffuse scattering and the scattering-length autocorrelation function is developed. The investigated models of coupling along the paracrystalline chain are the correlations between (i) the sizes of the scatterers, (ii) the sizes of scatterers and their separations, and (iii) the sizes of scatterers and the fluctuation of their separation distances. In the first case (i), the size of a scatterer is, on average, linked to that of its neighbors. As a result, a continuous transition from the total lack of size correlation (known as decoupling approximation or DA) to the scattering from monodisperse domains (local monodisperse approximation or LMA) is obtained. In the second case of correlation (ii), the mean interobject distance is assumed to depend on the respective sizes of nearest neighbors. Depending on the introduced correlation parameter, aggregation or hard-core-type effects can be accounted for. Surprisingly, in some cases, it is possible to find a peak in the scattering curve without any structure in the total interference function. The size–separation correlations may also dramatically reduce the scattering intensity close to the origin compared to the completely uncorrelated case. The last model (iii) foresees a coupling between the sizes of neighboring objects and the variance of the separation between neighbors. Within this model, on average along the chain, the fluctuations of distances between scatterers become dependent on the respective sizes of neighbors, while the mean distance between objects remains constant.

1. Introduction

Useful insights into the statistical properties of matter can be gained by carefully interpreting X-ray or neutron scattering patterns. For disordered systems, the analysis of the so-called diffuse scattering (Ziman, 1979; Welberry, 1985) requires the development of an appropriate model of disorder and a method for calculating the resulting scattering. However, the number of statistical parameters needed to characterize the disorder dramatically increases with the complexity of the studied system. In this context, simple analytical models of scattering can give an overview of the main phenomena. Using the theory of scattering from disordered crystalline systems, the aim of this work is to introduce, at the nodes of the well known Hosemann paracrystal model (Hosemann & Bagchi, 1962), scatterers whose scattering lengths display specific correlations from cell to cell. Our aim is to shed light on the specific signatures of such correlations in the scattered intensity.

In the general theory of scattering by matter, disordered or poorly crystalline systems (Guinier, 1956; Warren, 1969) can conveniently be described in terms of *substitution disorder* and *lattice disorder*. Substitution disorder consists of variations of the scatterers located at each lattice site, for instance different atomic species, molecule orientations, sizes of clusters *etc.* Lattice disorder involves variations of the site position away from that of a perfectly regular lattice; it can be divided into two kinds. The first kind corresponds to uncorrelated disorder and involves uncorrelated displacements of the lattice sites, thus keeping the long-range order and the sharpness of the Bragg peaks as long as an average periodic regular lattice can be defined. A well known example is the first-order Debye–Waller treatment of thermal vibrations, which reduces the diffraction peak intensities without any broadening, and homogeneously increases the diffuse background. The second kind of lattice disorder involves correlation between the displacements from site to site. Up to now, to describe it, two simple models, the *perturbed lattice* (Welberry *et al.*, 1980;

Welberry, 1985; Millane & Eads, 2000) and the *paracrystal* (Hosemann & Bagchi, 1962), have been developed. These models are well defined in one dimension (Mu, 1998; Millane & Eads, 2000) but their extensions to two or three dimensions are difficult (Welberry, 1985; Matsuoka *et al.*, 1987, 1990; Stroud & Millane, 1996; Busson & Doucet, 2000; Eads & Millane, 2000, 2001) and lead to unwanted properties like intense scattering at very small angles for the ideal paracrystal (Hosemann, 1951). This problem is circumvented either by analyzing the diffraction pattern in only one dimension of the reciprocal space or by arguing that the disorder in the system is fundamentally one-dimensional, like in layered structures. In the perturbed lattice, the displacements of the lattice nodes away from those of the perfect crystal are coupled from cell to cell through a joint normal probability. The main advantage is that the displacements are bounded; the scattering pattern is characterized by a peak broadening with scattering angle (Millane & Eads, 2000). The concept of the paracrystal was introduced for the first time by Hosemann in the early 50s (Hosemann, 1951) and extensively developed until the publication of a book (Hosemann & Bagchi, 1962). Its construction in one dimension relies on an intuitive growth process. Starting from an origin point, a paracrystalline chain is built in a sequential way by adding each site relative to its predecessor from the knowledge of the statistical distribution of distances between the lattice sites. The diffraction pattern resulting from this cumulative disorder is calculated taking advantage of the convolution products, the paracrystal being fundamentally defined through the statistics of the vectors joining lattice sites. The paracrystal has been widely used to analyze numerous types of scattering data ranging from polymer materials (Vignaud *et al.*, 1997) or disordered alloys to particle systems (Hosemann & Hindeleh, 1995; Metzger *et al.*, 1998). However, in the field of scattering from disordered or poorly crystallized material, distinguishing between substitution and lattice disorder is arbitrary since some degree of substitution at lattice sites can induce large lattice disorder. An intuitive case is that of a growth process, which involves hard-core repulsion between different species: the larger the species the farther away from its neighbors. The present theoretical work was indeed motivated by experimental results of grazing-incidence small-angle X-ray scattering (GISAXS) from growing disordered islands on surfaces (Renaud *et al.*, 2003; Revenant *et al.*, 2004). During the growth and coalescence processes, it seems that the Voronoi polyhedron associated with each particle scales with the radius of the central island, leading to a peculiar signature in the scattered signal below the correlation peak. Another example of coupling would be a layered structure with an alternate stacking of layers with different scattering factors and fluctuating thicknesses. In the field of surface science, an equivalent problem is encountered with scattering from terraces on vicinal surfaces (Croset & de Beauvais, 1997, 1998). In these examples, the resulting paracrystalline characteristics of the lattice-site positions are intimately linked to the sizes of the species that occupy the lattice nodes. This 'size–separation-distance coupling', as it will be called in the following, leads to specific features in the scattering pattern.

The interplay between substitution disorder and lattice disorder of the second kind has been clearly developed in many standard books on X-ray or neutron scattering (Guinier, 1956; Warren, 1969). However, the treatment is quite formal and practical examples or analytical models are still missing to characterize such a coupling. The aim of this work is to combine these two types of disorders within the framework of the paracrystal theory, thus taking into account the correlation between the scattering weights of the contents of the elementary cell and the lattice-site positions. The model is restricted to one dimension to allow for an analytical treatment. Although real systems are three-dimensional, scattering from disordered materials can often be recorded along a peculiar direction of reciprocal space and the diffraction pattern can thus be analyzed in terms of a one-dimensional model. Most of the time, this approximation is sufficiently accurate if not exact in some cases like reflectivity from layer stacking. As regards the small-angle scattering on particle systems, the data analysis often relies on simple assumptions, such as a direct interpretation of the position of the first intensity maximum, called the 'correlation peak', as being inversely proportional to the average nearest-neighbor distance or, when no correlation peak is present, as a simple relationship between the average particle size and the low wavevector transfer limit (Guinier gyration radius). This work shows that, when correlations between neighbors are present, these simple interpretations are no longer valid and an in-depth investigation of all the scattering curve has to be done, with sometimes no clear distinction between coherent scattering, *i.e.* the 'correlation peak', and diffuse scattering.

This article is written as follows. The general theory to calculate the diffuse scattering from the autocorrelation function accounting for any type of correlations is presented in §2. Apart from the obvious uncorrelated chain described in §3.3, three cases of correlations between the scatterers along the chain are considered: correlations between (i) sizes (§3.4), (ii) sizes and separation distance (§3.5), (iii) sizes and fluctuation of separation distance (§3.6); 'sizes' is a generic term for the scattering length of the unit-cell content. To proceed in the calculation of the scattering, correlations are restricted to first neighbors and the content of each cell is an object with either a Dirac shape or a stick shape whose scattering weight fluctuates from cell to cell. In each case (i), (ii), (iii), the effects of the introduced correlations on the scattering curve and on the autocorrelation function are detailed; peculiar attention is paid to the behavior of the maximum of intensity (the so-called 'correlation peak' in disordered systems) and to the Guinier region at small wavevector transfer. §3.4 details the effects of a correlation between the sizes of the neighboring particles, the paracrystalline lattice disorder being unaffected. This means that the size of a particle is linked, on average, to that of its neighbors through the correlation coefficient ρ ($|\rho| < 1$) of a normal law. The resulting coupling between neighbors separated by $n - 2$ other objects decreases as $|\rho|^n$. This model yields a continuous transition between the

complete lack of correlation known in the literature as the decoupling approximation (DA, $\rho = 0$) and the scattering from monodisperse domains, known as the local monodisperse approximation (LMA, $\rho = 1$); DA and LMA are the two main approximations used to analyze small-angle scattering from particles (Pedersen *et al.*, 1997; Pedersen, 1997; Lazzari, 2002; Revenant *et al.*, 2004). As the coupling parameter $0 < \rho < 1$ increases, the Bragg peak strengthens and the diffuse intensity in between decreases. The case $-1 < \rho < 0$ corresponding to an alternation of objects with small and large scattering weights leads to a pseudo-doubling of the periodicity. In the next sections, a nearest-neighbor correlation is introduced between the sizes of the scatterers and the two characteristic parameters of the paracrystal: the separation between sites and the fluctuations (more precisely the variance) of the distance between objects. In other words, during the build-up of the autocorrelation function of the paracrystalline chain, the statistical choice of the position of an object becomes dependent on the sizes of its neighbors. The coupling between size and separation distance, chosen linear, is an effective way to mimic attractive or repulsive interactions between large or small particles (depending on the value of the introduced correlation parameter α). The first intensity peak is found to shift towards the origin with the coupling parameter $|\alpha|$, with a maximum position which is thus no longer simply related to the nearest-neighbor separation distance D. Indeed, variation of α corresponds to a continuous transition between correlated objects with a clear peak in the interference function to uncorrelated objects with a flat interference function. The last coupling between the neighbor sizes and the variance of their separation distance (§3.6) induces a slight shift and a broadening of the correlation peak associated with a continuous increase of intensity close to the origin.

2. Scattering from one-dimensional paracrystals with correlations between scatterers: general theory

2.1. Autocorrelation function and diffuse scattering

Let us consider, along the x axis, an infinite one-dimensional chain of objects A_n, labeled by an index n from an arbitrary origin, whose scattering lengths or shape factors $\mathcal{F}(x, R_n)$ depend on a continuous parameter R_n. Typically, R_n can be the size of the scattering entity. However, this does not exclude the more general cases of genuine substitution disorders between different species or fluctuations of scattering lengths. R_n is assumed to be statistically distributed according to a probability density $p(R_n)$. The autocorrelation function $z(x)$ of the chain scattering length is calculated stepwise from (i) the statistical distribution $\mathcal{P}(d_n/[R_0, \ldots, R_n])$ of the distance d_n between A_{n-1} and A_n (d_n being algebraic) and in particular its dependence on the nature of the previous scatterers in the chain $(R_0, \ldots, R_n)$ and (ii) the joint probability $p(R_0, \ldots, R_n)$ of having a sequence $(R_0, \ldots, R_n)$. This joint probability is linked to the conditional probability $p(R_n/[R_0, \ldots, R_{n-1}])$ of having R_n knowing the $(R_0, \ldots, R_{n-1})$ sequence occurrence through

$$p(R_0, \ldots, R_n) = p(R_0)p(R_1/R_0)\ldots p(R_n/[R_0, \ldots, R_{n-1}]). \quad (1)$$

To build a representation of the chain, an object A_0 of size R_0 chosen with a probability $p(R_0)$ is first selected to be at the origin. Then, after R_1 has been chosen with a probability $p(R_1/R_0)$, the first neighbor A_1 of A_0 has a probability $\mathcal{P}(d/[R_0, R_1])$ to be at a distance d from A_0. The probability of putting the third object A_2 at a distance d from A_0 is equal to the product of the probability of having a distance d' between A_0 and A_1 {knowing the sizes of A_0 and A_1, *i.e.* $\mathcal{P}(d'/[R_0, R_1])$} by that of having a distance $d - d'$ between A_1 and A_2 {knowing the sizes of A_0, A_1 and A_2, *i.e.* $\mathcal{P}(d - d'/[R_0, R_1, R_2])$} integrated over all the possible distances d'. This probability is nothing else than the convolution product of the previously mentioned probabilities. Hence, the scattering-length autocorrelation function per object for $x > 0$, $z_+(x)$, is built step by step, by folding the A_0, A_n ($n = 1, \ldots, +\infty$) form factors with the above distance probabilities and by integrating the obtained convolution products over the size distributions:

$$\begin{aligned} z_+(x) = {} & \int p(R_0)\{\mathcal{F}(-y, R_0) \otimes \mathcal{F}(y, R_0) \otimes \delta(y)\}(x)\, \mathrm{d}R_0 \\ & + \iint p(R_0, R_1)\{\mathcal{F}(-y, R_0) \otimes \mathcal{F}(y, R_1) \\ & \otimes \mathcal{P}(y/[R_0, R_1])\}(x)\, \mathrm{d}R_0\, \mathrm{d}R_1 + \iiint p(R_0, R_1, R_2) \\ & \times \{\mathcal{F}(-y, R_0) \otimes \mathcal{F}(y, R_2) \otimes \mathcal{P}(y/[R_0, R_1]) \\ & \otimes \mathcal{P}(y/[R_0, R_1, R_2])\}(x)\, \mathrm{d}R_0\, \mathrm{d}R_1\, \mathrm{d}R_2 + \ldots \end{aligned} \quad (2)$$

$\otimes$ points out the convolution product in space. The total autocorrelation function $z(x)$ is given by

$$z(x) = z_0 + z_+(x) + z_-(x), \quad (3)$$

where $z_-(x) = z_+(-x)$ takes into account the contribution of objects located on the negative x axis; z_0 is the term linked to the autocorrelation function of the mean scattering length. The scattered intensity per object is then obtained by Fourier transform of equation (3):

$$I(q) = z_0\delta(q) + Z_+(q) + Z_-(q), \quad (4)$$

where q is the reciprocal-space coordinate. Obviously, $Z_-(q) = Z_+^*(q)$ where the asterisk $*$ indicates the complex conjugate. By introducing the object form factor $F(q, R_n)$, *i.e.* the Fourier transform of the object scattering length:

$$F(q, R_n) = \int_{-\infty}^{+\infty} \mathcal{F}(x, R_n) \exp(iqx)\, \mathrm{d}x \quad (5)$$

and the Fourier transform of each internode distance statistic:

$$P(q/[R_0, \ldots, R_n]) = \int_{-\infty}^{+\infty} \mathcal{P}(d/[R_0, \ldots, R_n]) \exp(iqd)\, \mathrm{d}d, \quad (6)$$

we find that the total scattered intensity reads

$$I(q) = z_0\delta(q) + \int p(R_0)|F(R_0, q)|^2\,\mathrm{d}R_0 + \iint p(R_0, R_1)F^*(q, R_0)F(q, R_1)P(q/[R_0, R_1])\,\mathrm{d}R_0\,\mathrm{d}R_1 + \iiint p(R_0, R_1, R_2)F^*(q, R_0)F(q, R_2)P(q/[R_0, R_1]) \times P(q/[R_0, R_1, R_2])\,\mathrm{d}R_0\,\mathrm{d}R_1\,\mathrm{d}R_2 + \ldots + \text{c.c.}, \quad (7)$$

where c.c. stands for the complex conjugate, which allows the cancelation of the imaginary part of the previous expression. The mean scattering length of the scatterers leads to the central peak $z_0\delta(q)$. If the chain has a finite size, the above expression has to be folded by the crystal shape form factor, *i.e.* the Fourier transform of its shape, which induces a broadening of the $q = 0$ Dirac peak. This first term is dropped in the following as the only structural information in $z(x)$ is contained in the oscillating part around z_0. All the effects of correlations in the scattering pattern are included in the joint probabilities $p(R_0, \ldots, R_n)$ (size–size coupling) and the $P(q/[R_0, \ldots, R_n])$ (size–separation coupling) terms.

2.2. Total and partial interference functions

Statistical information on the distribution of nodes is readily available within this model. Indeed, replacing by a Dirac peak the object shape $\mathcal{F}(x, R)$ and by one the form factor $F(x, R)$ and z_0 in equations (2)–(3) and (7), respectively, yields the node–node pair correlation function $g(x)$ and its Fourier transform, the total interference function $S(q)$. $g(x)$ is the reduced probability density of finding two objects separated by a distance x, irrespective of their sizes. For an in-depth study, the reduced node–node partial pair correlation functions $g_{\ell m}(x)$ can be obtained. They give the probability of finding an object of size R_m at a distance x from a central particle of size R_ℓ. In this article, the Faber–Ziman definition (Waseda, 1980) of the partial interference function $S_{\ell m}(q)$, which is the Fourier transform of $g_{\ell m}(x)$, is used:

$$I(q) = z_0\delta(q) + \Phi_0(q) + \iint p(R_\ell)p(R_m)F^*(q, R_\ell)F(q, R_m) \times S_{\ell m}(q)\,\mathrm{d}R_\ell\,\mathrm{d}R_m \quad (8)$$

$$\Phi_0(q) = \langle|F(q, R)|^2\rangle - |\langle F(q, R)\rangle|^2 \quad (9)$$

$$S_{\ell m}(q) = 1 + \rho_S \int [g_{\ell m}(x) - 1]\exp(-iqx)\,\mathrm{d}x. \quad (10)$$

The brackets $\langle\ldots\rangle$ denote the mean value over the size distribution and ρ_S is the linear density of objects. A comparison with equation (7) leads to:

$$S_{\ell m}(q) = 1 + \frac{1}{p(R_\ell)p(R_m)}\left\{p(R_\ell, R_m)P(q/[R_\ell, R_m]) + \int p(R_\ell, R, R_m)P(q/[R_\ell, R])P(q/[R_\ell, R, R_m])\,\mathrm{d}R + \iint p(R_\ell, R, R', R_m)P(q/[R_\ell, R])P(q/[R_\ell, R, R']) \times P(q/[R_\ell, R, R', R_m])\,\mathrm{d}R\,\mathrm{d}R' + \ldots + \text{c.c.}\right\} \quad (11)$$

As $S_{\ell m}(q) \underset{q\to+\infty}{\overset{q\to+\infty}{\simeq}} 1$ [see for instance equation (64)], it appears that $I(q) \underset{q\to+\infty}{\overset{q\to+\infty}{\simeq}} \langle|F(q, R)|^2\rangle$. Hence, the high-$q$ range of the diffuse scattering is only driven by the mean object form factor because of the loss of spatial long-range order induced by the underlying paracrystal.

3. Correlation effects on scattering from one-dimensional paracrystal chains

To go further, specific forms of the scattering length $\mathcal{F}(x, R)$ have to be chosen. Also, specific analytic correlation models are introduced in either the joint probability $p(R_0, \ldots, R_n)$ or in the $P(q/[R_0, \ldots, R_n])$ terms of equation (7). This allows us to evaluate the multiple integrals involved in equation (7) and, in some cases, to carry out their summation.

3.1. Scattering lengths or object shapes

Two simple and natural one-dimensional object shapes are considered.

(i) The point function or Dirac peak:

$$\mathcal{F}(x, R) = 2R\rho_0\delta(x)$$
$$F(q, R) = 2R\rho_0. \quad (12)$$

(ii) The stick:

$$\mathcal{F}(x, R) = \begin{cases}\rho_0 & \text{if } |x| \le R\\ 0 & \text{if } |x| > R\end{cases}$$
$$F(q, R) = 2R\rho_0[\sin(qR)/qR], \quad (13)$$

where ρ_0 is the constant density of scattering length.
These two shapes could, for instance, describe either the neutron scattering length of a nucleus or the one-dimensional shape of the electron cloud in X-ray scattering. They lead, respectively, to a constant value or a $1/q^2$ dependence of the scattered intensity in reciprocal space.

3.2. Distributions of scattering lengths and of distances

For the sake of simplicity, the scattering lengths or object sizes are assumed to follow a Gaussian probability law with the two first centered moments $\overline{R}$ and σ_R^2:

$$p(R) = \frac{1}{\sigma_R(2\pi)^{1/2}}\exp\left[-\frac{(R-\overline{R})^2}{2\sigma_R^2}\right]. \quad (14)$$

For the Dirac-shape case, this leads to

$$\langle|F(q, R)|^2\rangle = 4\rho_0^2(\overline{R}^2 + \sigma_R^2), \quad |\langle F(q, R)\rangle|^2 = 4\rho_0^2\overline{R}^2; \quad (15)$$

and for the stick case:

$$\langle|F(q, R)|^2\rangle = \frac{2\rho_0^2}{q^2}[1 - \exp(-2\sigma_R^2q^2)\cos(2q\overline{R})] \quad (16)$$

$$|\langle F(q, R)\rangle|^2 = \frac{4\rho_0^2}{q^2}\sin^2(q\overline{R})\exp(-q^2\sigma_R^2). \quad (17)$$

The $\mathcal{P}(d_n/[R_0, \ldots, R_n])$ probability is chosen such that its first moment, *i.e.* the average separation between neighboring objects, is constant and equal to D:

$$\int\ldots\int d_n\mathcal{P}(d_n/[R_0, \ldots, R_n])\,\mathrm{d}R_0\ldots\mathrm{d}R_n\,\mathrm{d}d_n = D. \quad (18)$$

Its intrinsic second moment, *i.e.* without any correlations, is called σ_D. Thus, the linear object density is constant: $\rho_S = 1/D$ and $z_0 = 4\rho_S\rho_0^2\overline{R}^2$.

In all the following simulations, the same numerical parameters will be used to highlight the main characteristic features of correlations on scattering:

$$\rho_0 = 1, \quad \overline{R} = 5, \quad \sigma_R = 0.4\overline{R} = 2, \quad D = 3.4\overline{R} = 17, \quad \sigma_D = 0.1D = 1.7. \tag{19}$$

The paracrystal statistics will be chosen as Gaussian and the $I_0 = 4\rho_0^2\overline{R}^2$ value will often be used for normalization.

3.3. One-dimensional paracrystal without correlation: the decoupling approximation

If there is no correlation between neighboring objects:

(i) the joint probability of sizes is simply the product of the probabilities of having the sizes $R_0, \ldots, R_n$:

$$p(R_0, \ldots, R_n) = p(R_0) \ldots p(R_n); \tag{20}$$

(ii) the statistical distribution of the nearest-neighbor internode distance is independent of the object sizes:

$$\mathcal{P}(d_n/[R_0, \ldots, R_n]) = \mathcal{P}(d_n) = \mathcal{P}(d). \tag{21}$$

A Gaussian probability of internode spacing would give

$$\mathcal{P}(d) = \frac{1}{\sigma_D(2\pi)^{1/2}} \exp\left[-\frac{(d-D)^2}{2\sigma_D^2}\right]$$
$$P(q) = \exp\left(-\frac{q^2\sigma_D^2}{2}\right)\exp(iqD). \tag{22}$$

With these hypotheses, known as the decoupling approximation (Guinier & Fournet, 1955; Guinier, 1956), writing $P(q) = \phi(q)\exp(iqD)$, the scattered intensity reads

$$I(q) = \int p(R)|F(q,R)|^2\,\mathrm{d}R + 2\left|\int p(R)F(q,R)\,\mathrm{d}R\right|^2 \times \sum_{n=1}^{+\infty}\phi(q)^n\cos(nqD). \tag{23}$$

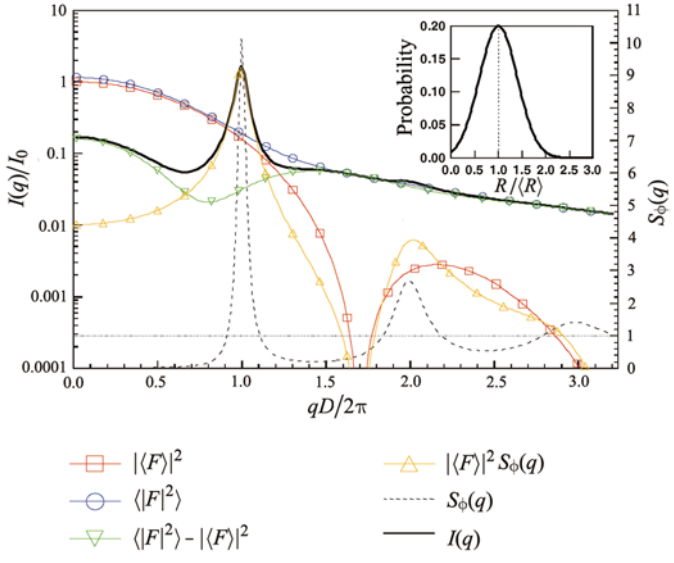

Figure 1
Scattered intensity $I(q)$, form factors $\langle|F(q)|^2\rangle$, $|\langle F(q)\rangle|^2$, interference function $S_\phi(q)$ (right scale), and coherent $|\langle F(q)\rangle|^2 S_\phi(q)$ and diffuse scattering $\phi_0(q) = \langle|F(q)|^2\rangle - |\langle F(q)\rangle|^2$ of a Gaussian paracrystalline chain made of uncorrelated sticks, *i.e.* within the decoupling approximation [parameters of equation (19)]. The Gaussian stick size distribution is shown in the inset. The intensities have been normalized by $I_0 = 4\rho_0^2\overline{R}^2$.

Using the summation (77) of Appendix *A*, the interference function of a one-dimensional Hosemann paracrystal (Hosemann & Bagchi, 1962) appears:

$$S_\phi(q) = \frac{1-\phi(q)^2}{1+\phi(q)^2-2\phi(q)\cos(qD)}. \tag{24}$$

The scattered intensity can then be decomposed into the sum of a coherent term,

$$I(q) = \Phi_0(q) + |\langle F(q,R)\rangle|^2 S_\phi(q), \tag{25}$$

and an incoherent one linked to the size distribution of scatterers along the chain,

$$\Phi_0(q) = \langle|F(q,R)|^2\rangle - |\langle F(q,R)\rangle|^2. \tag{26}$$

The high-q limit of the interference function $S_\phi(q) \to 1$ is linked to the loss of long-range order in the chain due to cumulative paracrystalline disorder; $S_\phi(q)$ shows broader and broader successive maxima at Bragg positions, *i.e.* at integer values of $qD/2\pi$. When $\sigma_D \to 0$, the perfect crystal is recovered. Fig. 1 illustrates the DA for stick objects. With the chosen parameters, the diffuse term $\Phi_0(q)$ dominates the scattering curve except close to the first maximum of the interference function where all the intensity is concentrated in the coherent scattering term. Notice the significant difference between the $\langle|F(q,R)|^2\rangle$ and $|\langle F(q,R)\rangle|^2$ mean values.

3.4. Size–size correlations: from the decoupling approximation to the local monodisperse approximation

3.4.1. General approach. The size–size correlation is the first type of correlation considered herein. The size of an object is assumed to depend on those of its neighbors, whereas the internode distances obey the same law $\mathcal{P}(d)$ all along the chain (*i.e.* there is no size–separation correlation). After summation over the intermediate variables $R_1, \ldots, R_{n-1}$, equation (7) reduces to

$$I(q) = \langle|F(q,R)|^2\rangle + 2\sum_{n=1}^{+\infty}\left[\iint p(R_0)p(R_n/R_0)F^*(q,R_0) \times F(q,R_n)\,\mathrm{d}R_0\,\mathrm{d}R_n\right]\phi^n(q)\cos(nqD). \tag{27}$$

In order to highlight the difference between equation (27) and the case without correlation [equation (25)], equation (27) can be rewritten as

$$I(q) = |\langle F(q,R)\rangle|^2 S_\phi(q) + \Phi_0(q) + I_c(q)$$
$$I_c(q) = 2\sum_{n=1}^{+\infty}\Phi_n(q)\phi^n(q)\cos(nqD). \tag{28}$$

$I_c(q)$ contains all the effects of the coupling between scatterer sizes. Each $\Phi_n(q)$ coefficient describes the correlations of the centered scattered amplitudes between two objects separated by n nodes:

$$\Phi_n(q) = \left\langle [F(q, R_n) - \langle F(q, R)\rangle][F(q, R_0) - \langle F(q, R)\rangle]^* \right\rangle$$
$$= \iint p(R_0)p(R_n/R_0)F^*(q, R_0)F(q, R_n)\,\mathrm{d}R_0\,\mathrm{d}R_n - \left|\int p(R)F(q, R)\,\mathrm{d}R\right|^2. \quad (29)$$

3.4.2. The normally distributed Markov chain with correlation to first neighbor. To go further, an expression of $p(R_0, \ldots, R_n)$ is needed. A simple Markov chain, restricted to first-neighbor interactions, is considered:

$$p(R_0, \ldots, R_n) = p(R_0, R_1)\ldots p(R_{n-1}, R_n). \quad (30)$$

The sizes R_n are assumed to be normally distributed [equation (14)] and the joint distribution of the sizes of two neighboring objects is assumed to be normal, *i.e*:

$$p(R_{n-1}, R_n) = \frac{1}{2\pi\sigma_R^2(1-\rho^2)^{1/2}} \times \exp\left[-\frac{\Delta R_{n-1}^2 + \Delta R_n^2 - 2\rho\Delta R_{n-1}\Delta R_n}{2\sigma_R^2(1-\rho^2)}\right], \quad (31)$$

where $\Delta R_n = R_n - \overline{R}$, $\sigma_R = (\langle \Delta R_n^2\rangle)^{1/2}$ is the standard deviation of the size from the mean value $\overline{R}$ and ρ is a correlation coefficient:

$$\rho = \frac{\langle \Delta R_{n-1}\Delta R_n\rangle}{\sigma_R^2}. \quad (32)$$

The conditional probability can easily be deduced from equations (14) and (30):

$$p(R_n/R_{n-1}) = \frac{p(R_{n-1}, R_n)}{p(R_{n-1})} = \frac{1}{\sigma_R(1-\rho^2)^{1/2}(2\pi)^{1/2}}\exp\left[-\frac{(\Delta R_n - \rho\Delta R_{n-1})^2}{2\sigma_R^2(1-\rho^2)}\right]. \quad (33)$$

A useful and interesting property of the normal distribution is that the correlation between two objects, spaced by n internodes, decreases as ρ^n. Indeed, using equation (33), it can be demonstrated recursively that

$$p(R_n/R_0) = \iint p(R_1/R_0)\ldots p(R_n/R_{n-1})\,\mathrm{d}R_1\ldots\mathrm{d}R_{n-1} = \frac{1}{\sigma_R(1-\rho^{2n})^{1/2}(2\pi)^{1/2}}\exp\left[-\frac{(\Delta R_n - \rho^n\Delta R_0)^2}{2\sigma_R^2(1-\rho^{2n})}\right]. \quad (34)$$

$|\rho| < 1$ ensures the fact that the chain is stationary [equation (14)], *i.e.*

$$\lim_{n\to+\infty} p(R_n/R_0) = p(R_n). \quad (35)$$

3.4.3. Correlation limit cases. It is shown below that, without any assumption on the shape of the object, the two usual approximations, DA and LMA, correspond to the limit cases $\rho = 0$ and $\rho = 1$, respectively. A numerical representation of this chain is given in Fig. 2 for various correlation coefficients ρ. Without correlation, $\rho = 0$, $\Phi_n(q) = 0$ for $n = 1, \ldots, +\infty$: the decoupling approximation [equations (25)–(26)] is recovered. For increasingly positive ρ values, the objects tend to be locally all of the same size. For ρ close to 1, from a scattering point of view the situation corresponds to an incoherent interference between domains in which all objects have the same scattering length, *i.e.* are monodisperse. Indeed, for $\rho = 1$, equation (34) shows that

$$\lim_{\rho\to1} p(R_n/R_0) = \delta(\Delta R_n - \Delta R_0)$$
$$\lim_{\rho\to1} \Phi_n(q) = \Phi_0(q). \quad (36)$$

Thus, within this limit, the scattered intensity (27) is

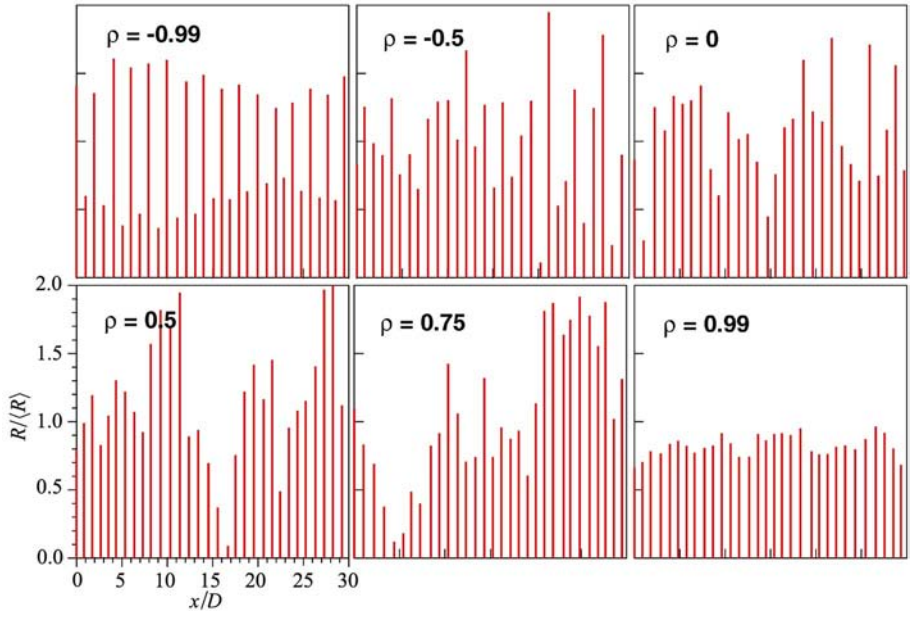

Figure 2
A representation of the normally distributed Markov chain for various first-neighbor size–size correlation coefficients ρ. The size disorder is $\sigma_R = 0.4\overline{R}$ [parameters of equation (19)].

$$\lim_{\rho\to 1} I(q) = \langle |F(q,R)|^2 \rangle S_\phi(q), \tag{37}$$

which is known as the local monodisperse approximation. This equation is often used to analyze experimental data of scattering from particles (Pedersen, 1994; Pedersen *et al.*, 1997; Lazzari, 2002), thus implicitly assuming that the sample is made of monodisperse domains over the coherent length of the beam. Such a hypothesis is clearly unphysical in many situations (Revenant *et al.*, 2004). At the opposite limit $\rho = -1$, the more or less monodisperse domains of the chain are made of doubled unit cells (Fig. 2). In this limit,

$$\begin{aligned} \lim_{\rho\to -1} p(R_{2n}/R_0) &= \delta(\Delta R_{2n} - \Delta R_0) \\ \lim_{\rho\to -1} p(R_{2n+1}/R_0) &= \delta(\Delta R_{2n+1} + \Delta R_0) \end{aligned} \tag{38}$$

and

$$\begin{aligned} &\lim_{\rho\to -1} \Phi_{2n}(q) = \Phi_0(q) \\ &\lim_{\rho\to -1} \Phi_{2n+1}(q) = \Phi_\pm(q) = \big\langle [F(q,\overline{R}+\Delta R_0) - \langle F(q,R)\rangle] \\ &\qquad \times [F(q,\overline{R}-\Delta R_0) - \langle F(q,R)\rangle]^* \big\rangle. \end{aligned} \tag{39}$$

The two involved summations [equations (78)–(79)] over n of equation (28) give the limit of the correlation scattering term $I_c(q)$:

$$\lim_{\rho\to -1} I_c(q) = 2\frac{\Phi_0(q)\phi^2(q)[\cos(2qD) - \phi^2(q)] + \Phi_\pm(q)\phi(q)[1-\phi^2(q)]}{1+\phi^4(q) - 2\phi^2(q)\cos(2qD)}.$$

3.4.4. Specific object shapes. Let us now pursue the calculation with specific object shapes, namely the Dirac peak and the stick.

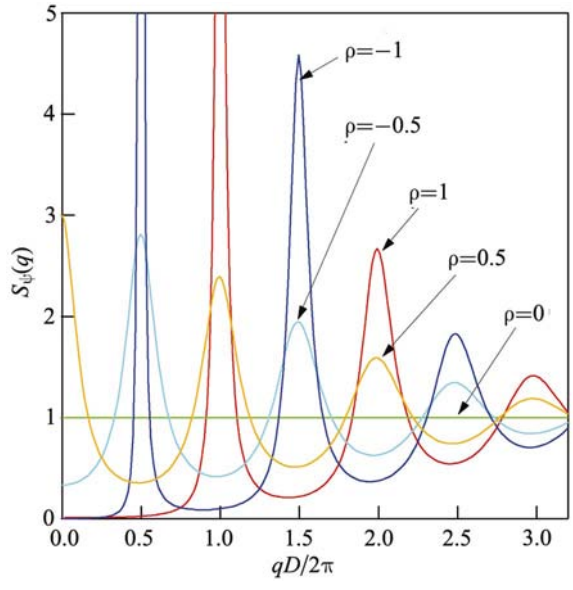

Figure 3
The $S_\psi(q)$ function [equation (41)] involved in the diffuse scattering term for Dirac peak objects. The chosen statistic for the paracrystal is Gaussian [equation (22)] with $\sigma_D = 0.1D$.

The Dirac peak case

If the objects are Dirac like, using equations (12) and (34), the integral involved in the $\Phi_n(q)$ coefficient of equation (29) is easily calculated for normally distributed variables using the variable change ($u = \Delta R_0$, $v = \Delta R_n - \rho^n \Delta R_0$): $\Phi_n(q) = 4\rho_0^2\sigma_R^2\rho^n$. The geometric sum in equation (28) leads to the following scattered intensity:

$$\begin{aligned} I(q) &= 4\rho_0^2\overline{R}^2 S_\phi(q) + \phi_0(q) + I_c(q) \\ I_c(q) &= 4\rho_0^2\sigma_R^2[S_\psi(q) - 1] \\ \phi_0(q) &= 4\rho_0^2\sigma_R^2, \end{aligned} \tag{40}$$

where

$$S_\psi(q) = \frac{1-\psi(q)^2}{1+\psi(q)^2 - 2\psi(q)\cos(qD)} \quad \text{with} \quad \psi(q) = \rho\phi(q). \tag{41}$$

The term $\Phi_\pm(q)$ can also be evaluated:

$$\Phi_\pm(q) = -4\rho_0^2\sigma_R^2. \tag{42}$$

The diffuse scattering function $S_\psi(q)$, which is quite analogous to the interference function of the paracrystal equation (24), is shown in Fig. 3 for various correlation parameters. For positive ρ values, a strengthening of the scattered intensity is observed at Bragg values $qD = 2n\pi$ whereas peaks of diffuse scattering arise at anti-Bragg positions for negative values. For $\rho = 0$, $S_\psi(q) = 1$ and the DA limit is recovered.

The stick case

For objects in the form of sticks, by using the form-factor expressions (16)–(17), the double integral involved in equation (29) can be calculated analytically:

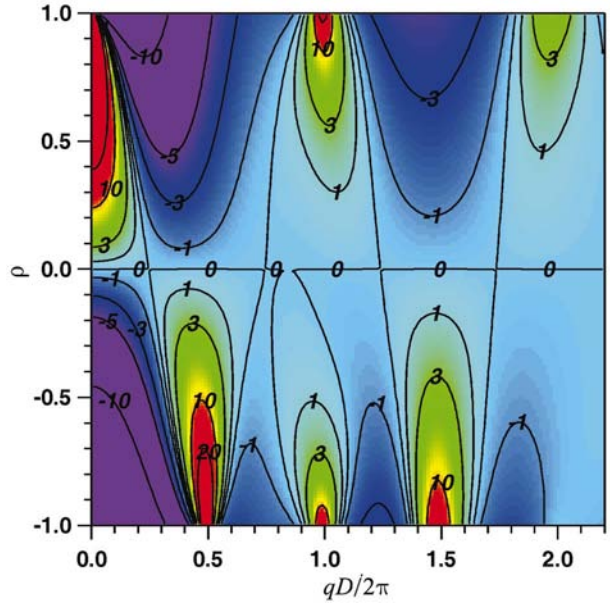

Figure 4
The correlation scattering term $I_c(q)/I_0$ [equation (28)] for a Markov chain of normally distributed sticks as a function of the correlation coefficient ρ (see text). $I_0 = 4\rho_0^2\overline{R}^2$ is used as a normalization value. Isolines ($\times 100$) give the linear color scale. The parameters used are those of equation (19).

$$\Phi_n(q) = \frac{4\rho_0^2}{q^2}\exp(-q^2\sigma_R^2)\{[(\cosh(q^2\sigma_R^2\rho^n) - 1]\sin^2(q\overline{R}) + \sinh(q^2\sigma_R^2\rho^n)\cos^2(q\overline{R})\}. \quad (43)$$

The $\Phi_{\pm}(q)$ term is also available:

$$\Phi_{\pm}(q) = \frac{2\rho_0^2}{q^2}[\exp(-2q^2\sigma_R^2) - \cos(2q\overline{R}) - 2\sin^2(q\overline{R})\exp(-q^2\sigma_R^2)]. \quad (44)$$

The correlation term $I_c(q)$ [equation (28)] is illustrated in Fig. 4. For increasingly positive values of the correlation coefficient ρ, the long-range correlation leads to a strengthening of intensity below the Bragg peaks and a decrease in between. For negative values, the same behavior is observed with a pseudo-doubling of the periodicity as has already been highlighted in Fig. 2. The latter is due to a cell content that consists on the average of a 'large' and a 'small' stick. This phenomenon is well illustrated in Fig. 5 on the total scattered intensity or on the scattering-length autocorrelation function $z(x)$, which is calculated by back-Fourier transform of $I(q)$. At $\rho = 0$, with the chosen parameters, only one scattering peak appears in the coherent term of equation (25) and $I_c(q) = 0$. With increasing ρ, the peak gets narrower and the diffuse background decreases. This illustrates the arbitrary distinction between coherent and diffuse scattering. It is worth noticing the large intensity difference between positive and negative ρ values at small q values. An increase of the scattered intensity is observed for $\rho > 0$, whereas the low-q scattering for $\rho < 0$ is weaker due to damping of long-range density fluctuations. This can be illustrated on a simple example: the nearest neighbor of a 'large' stick is statistically a 'small' one which immediately compensates for the increase of density. This is all the more true as ρ is close to -1. The observed damped oscillatory behavior in Fig. 5 and the subsequent loss of long-range order result from a mixture of paracrystal and size disorders. The larger the correlation coefficient ρ, the slower the convergence towards the limit value z_0. As an example at $\rho = 0.75$, the correlation term $I_c(q)$ of equation (28) is expanded in Fig. 6 along its different components $\Phi_n(q)$, which are a fingerprint of the correlation to the nth neighbor. The increase of the oscillatory behavior for high n values leads to destructive interferences, except close to the Bragg positions where all the terms are in phase and thus strengthens the intensity.

3.4.5. Limit at small wavevector transfer. As $\lim_{q\to 0}\phi(q) = 1 - q^2\sigma_D^2/2$, the $q = 0$ limit of the scattered intensity is in both cases (Dirac and stick objects) given by the expression:

$$\lim_{q\to 0}\frac{I(q)}{\rho_0^2} = 4\overline{R}^2\left(\frac{\sigma_D}{D}\right)^2 + 4\sigma_R^2\frac{1+\rho}{1-\rho}. \quad (45)$$

This indicates the generality of the low-q-range intensity behavior. One has to keep in mind that the central Dirac peak due to the mean scattering length was excluded on purpose. Thus, this limit is entirely due to the fluctuations of the scattering length in the probed volume (Guinier & Fournet, 1955; Guinier, 1956; Ziman, 1979), either due to the fluctuations of the number of paracrystal lattice nodes or to the fluctuations of the object sizes. The value $I(q = 0)$ diverges when $\rho = 1$ because the coherence length of the monodisperse domains measured by the inverse of the $I(q = 0)$ peak width increases. This behavior is characteristic of long-range fluctuations encountered close to a critical point. The limit $\rho = -1$ yields a minimum of diffuse scattering at $q = 0$ as no long-range density fluctuation is expected because each local fluctuation is immediately canceled by its first neighbors.

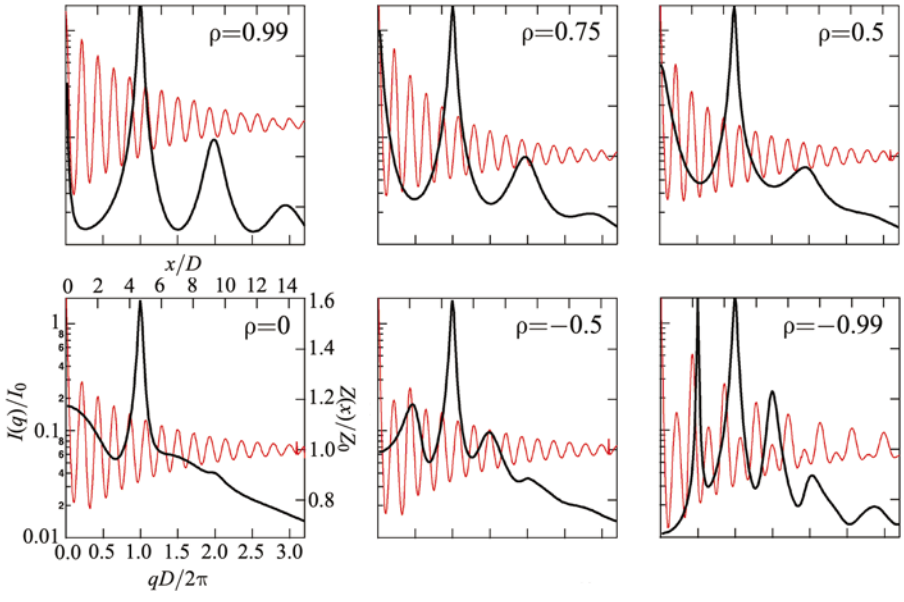

Figure 5
Total scattered intensity $I(q)/I_0$ (thick line) [equation (28)] and scattering-length autocorrelation function $z(x)/z_0$ (thin line) of a one-dimensional stick chain. The stick sizes are correlated to first neighbor following a joint normal law and the paracrystal statistic used is Gaussian [equation (22)]. The numerical parameters are given in equation (19).

3.5. Correlations between sizes and the separation distance: effects of aggregation and hard-core repulsion on scattering

3.5.1. General approach. In this section, the coupling between sizes and separation of the scatterers is considered. The object sizes are assumed to be uncorrelated [equation (20)] but the separation between an object A_n and its previous neighbor A_{n-1} is supposed to depend on the respective sizes of the previous objects in the chain. The simplest dependence that fulfills symmetry rules is a linear one to first neighbors:

$$\int_{-\infty}^{+\infty} d_n \mathcal{P}(d_n/[R_0, \ldots, R_n])\, \mathrm{d}d_n = D + \alpha(\Delta R_{n-1} + \Delta R_n), \quad (46)$$

which corresponds to

$$P(q/[R_0, \ldots, R_n]) = \phi(q) \exp(iqD) \exp[i\alpha q(\Delta R_{n-1} + \Delta R_n)]. \quad (47)$$

The dependence of equation (46) conveys a kind of hard-core effect, in particular if $D > 2\overline{R}$ and $\alpha > 1$. However, within this model, the object overlapping is possible, except if the paracrystal law of equation (46) is explicitly defined only for positive $d_n - R_{n-1}$, as with the gamma law for instance. Averaging over the sizes of the neighboring particles in equation (47) shows that the mean internode distance is still equal to D and its centered variance is σ_D^2. A representation of the chain obtained by following this construction rule is given in Fig. 7 for a Gaussian paracrystal. Even if the linear density of objects is constant whatever the coefficient α is, a clear aggregation phenomenon is observed for 'small' or 'large' sticks. To highlight this point, a criterion of aggregation for sticks needs to be defined for the gap between particles as illustrated in the insets of Fig. 7. As $\langle d_n \rangle - R_n - R_{n+1}$ is the average gap between two particles of sizes R_n, R_{n+1}, the normalized average gap $\widetilde{g_n}$ is defined as

$$\widetilde{g_n} = \frac{\langle d_n \rangle - R_n - R_{n+1}}{D - 2\overline{R}} = \frac{D - 2\overline{R}\alpha}{D - 2\overline{R}} + \frac{2\overline{R}(\alpha - 1)}{D - 2\overline{R}} \left[\frac{R_n + R_{n+1}}{2\overline{R}}\right]. \quad (48)$$

On the average, two neighboring particles tend to aggregate when $\widetilde{g_n} < 0$. A specific value of α has to be considered: $\alpha_0 = D/2R$. In this case, the normalized gap $\widetilde{g_n} = (R_n + R_{n+1})/2\overline{R}$ scales with the size of the objects: the system

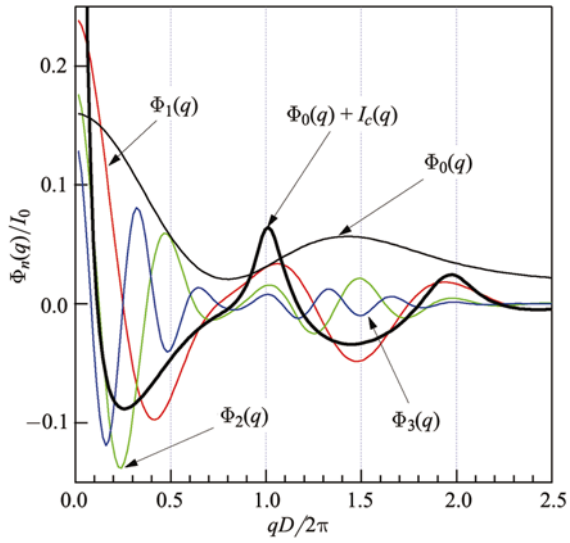

Figure 6
The different components $\Phi_n(q)\cos(nqD)\exp(-nq^2\sigma_D^2)$ of the correlation term $I_c(q)$ at $\rho = 0.75$ [equation (28)] for sticks whose sizes are correlated to first neighbors. Same parameters as in Fig. 5.

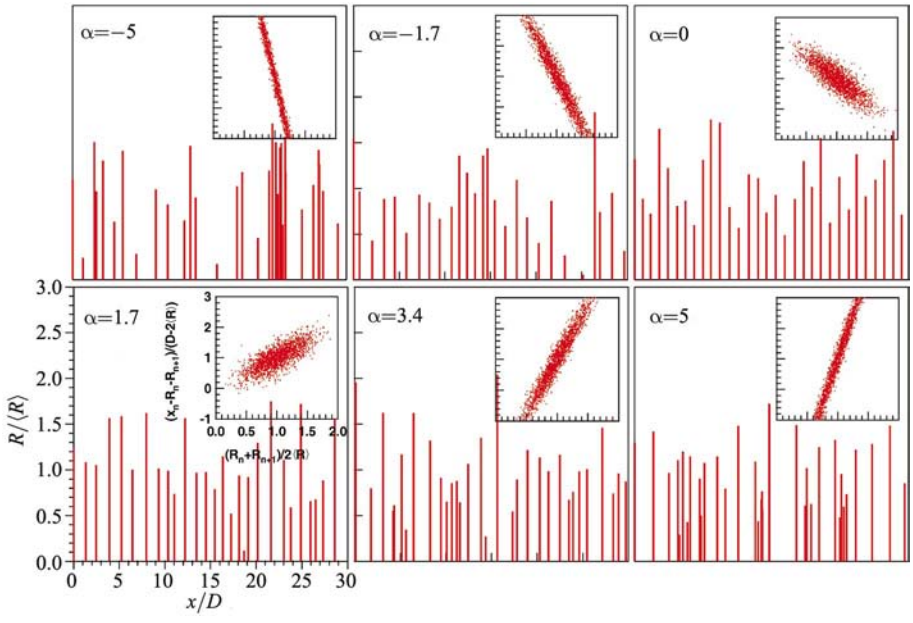

Figure 7
A representation of the chain for various correlation parameters α between the mean internode distance and the object sizes [equation (46)]. The object sizes are distributed according to a Gaussian law $\sigma_R = 0.4\overline{R}$. The paracrystal statistics are also Gaussian with $\sigma_D = 0.1D$. The insets show a sampling of the gap between objects $\widetilde{g_n} = (\langle d_n \rangle - R_n - R_{n+1})/(D - 2\overline{R})$ *versus* the sum of the size of two neighboring particles $(R_n + R_{n+1})/2\overline{R}$. Note that $\alpha_0 = D/2\overline{R} = 1.7$.

is scale invariant and, as a consequence, it is impossible to distinguish between areas consisting of large and small sticks. For $\alpha < \alpha_0$, the larger objects are closer to each other than the smaller ones, which 'repel' each other. On the other hand, for $\alpha > \alpha_0$, the larger objects are farther apart and the smaller ones tend to aggregate. If the $\alpha > \alpha_0$ case is intuitive for X-ray scattering where the scattering length is proportional to the size of the electronic cloud, the situation $\alpha < \alpha_0$ can be encountered in neutron scattering where the scattering length is not related to the size of the atoms but to the nucleus content. Note that $\alpha = 1$ leads to a constant gap $\widetilde{g}_n$ between the scatterers.

The total scattered intensity follows readily from equation (7):

$$I(q) = \langle |F(q, R)|^2 \rangle + \sum_{n=1}^{+\infty} I_c^n(q) + \text{c.c.}$$

$$I_c^n(q) = \phi^n(q) \exp(inqD) \int \ldots \int p(R_0) \ldots p(R_n) F^*(q, R_0) F(q, R_n) \times \exp\left[i\alpha q \left(\Delta R_0 + 2 \sum_{k=1}^{n-1} \Delta R_k + \Delta R_n \right) \right] \mathrm{d}R_0 \ldots \mathrm{d}R_n. \quad (49)$$

3.5.2. Specific object shapes.

The Dirac peak object

By using the form-factor expression of a Dirac object [equation (12)] for a Gaussian size distribution [equation (14)], the multiple integral in $I_c^n(q)$ reduces to

$$I_c^n(q) = 4\rho_0^2 \phi^n(q) \exp(inqD) \exp[-2\alpha^2 q^2 \sigma_R^2 (n - \tfrac{1}{2})][\overline{R} + i\alpha q \sigma_R^2]^2. \quad (50)$$

After the complex conjugate has been added, the summation of equation (49) reads

$$I(q) = 4\rho_0^2(\overline{R}^2 + \sigma_R^2) + 8\rho_0^2 \exp(\alpha^2 q^2 \sigma_R^2)(\overline{R}^2 + \alpha^2 q^2 \sigma_R^4) \times \sum_{n=1}^{+\infty} \psi(q)^n \cos[nqD + \xi_0(q)], \quad (51)$$

where the variables $\psi(q)$ and $\xi_0(q)$ are defined by

$$\psi(q) = \phi(q) \exp(-2\alpha^2 q^2 \sigma_R^2) \quad (52)$$

$$\tan[\xi_0(q)] = \frac{2\alpha q \overline{R} \sigma_R^2}{\overline{R}^2 - \alpha^2 q^2 \sigma_R^4}. \quad (53)$$

By applying the geometric sums of Appendix *A*, the previous sum can be handled analytically:

$$I(q) = 4\rho_0^2(\overline{R}^2 + \sigma_R^2) + 8\rho_0^2 \exp(\alpha^2 q^2 \sigma_R^2)(\overline{R}^2 + \alpha^2 q^2 \sigma_R^4) \times \frac{\psi(q) \cos[qD + \xi_0(q)] - \psi^2(q) \cos[\xi_0(q)]}{1 + \psi^2(q) - 2\psi(q) \cos(qD)}. \quad (54)$$

The stick object

This approach is similar to the Dirac-like object case, except for the form factor which comes into play in equation (13). The multiple integral of $I_c^n(q)$ in equation (49) is calculated in a straightforward way by expanding the product $F(q, R_0)F(q, R_n) \propto \sin[q(\overline{R} + \Delta R_0)] \sin[q(\overline{R} + \Delta R_n)]$ in complex numbers:

$$I_c^n(q) = \frac{4}{q^2} \rho_0^2 \phi^n(q) \exp(inqD) \exp\{-[(2n-1)\alpha^2 + 1] q^2 \sigma_R^2\} \times [1 - \cos(2q\overline{R}) \cosh(2\alpha q^2 \sigma_R^2) + i \sin(2q\overline{R}) \sinh(2\alpha q^2 \sigma_R^2)]. \quad (55)$$

By introducing again

$$\psi(q) = \phi(q) \exp(-2\alpha^2 q^2 \sigma_R^2) \quad (56)$$

$$\tan[\xi_0(q)] = \frac{\sin(2q\overline{R}) \sinh(2\alpha q^2 \sigma_R^2)}{1 - \cos(2q\overline{R}) \cosh(2\alpha q^2 \sigma_R^2)} \quad (57)$$

and gathering each term with its complex conjugate, the summation of equation (54) reads

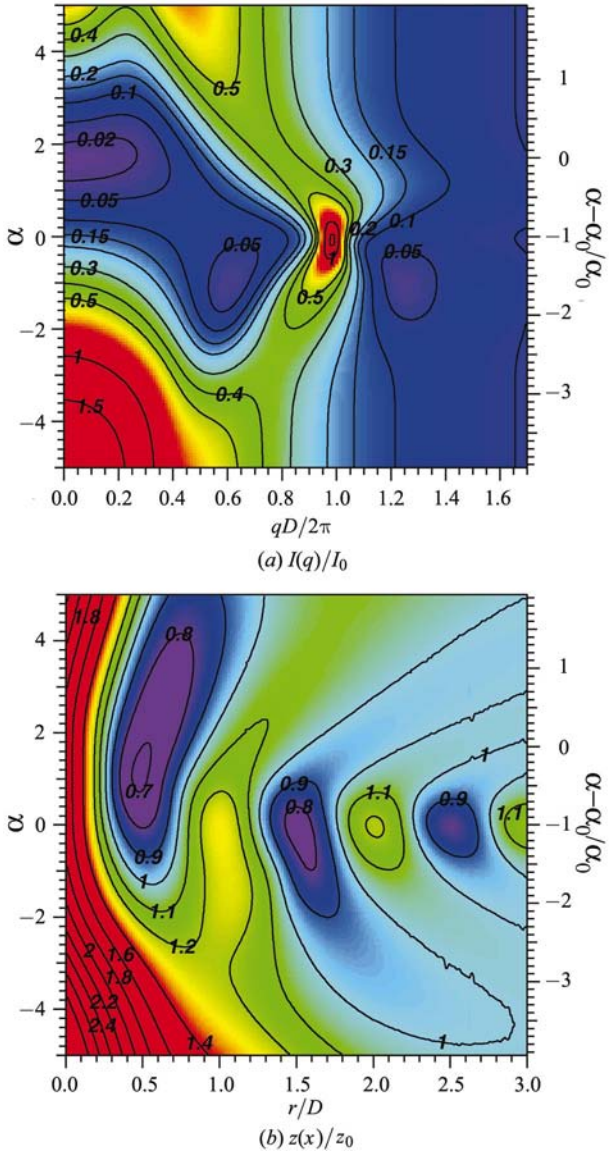

Figure 8
(*a*) A map in the (q, α) space of the total scattered intensity [equation (58)] by a chain made of sticks aggregated on a Gaussian paracrystal according to equation (46). The intensity is normalized by $I_0 = 4\rho_0^2 \overline{R}^2$ and the numerical parameters are given in equation (19). (*b*) A map of the associated scattering-length autocorrelation function, $z(x)/z_0$.

$$I(q) = \frac{2\rho_0^2}{q^2}[1 - \exp(-2\sigma_R^2 q^2)\cos(2q\overline{R})] + \frac{4\rho_0^2}{q^2}\exp[-(1-\alpha^2)q^2\sigma_R^2][\cosh(2\alpha q^2\sigma_R^2) - \cos(2q\overline{R})] \times \sum_{n=1}^{+\infty}\psi^n(q)\cos[nqD + \xi_0(q)]. \quad (58)$$

The above sum can be carried out with the help of Appendix *A* as in equation (51). It is easily checked that $I(q) = 0$ when the chain is made of contiguous sticks, *i.e.* $D = 2\overline{R}$, $\alpha = 1$; there remains only the scattering from the mean density, *i.e.* a Dirac peak at the origin.

The calculated scattered intensity using equation (58) is shown in Figs. 8–9 together with the corresponding scattering-length autocorrelation function. The maximum of intensity, located close to $q = 2\pi/D$ for $\alpha = 0$, shifts towards lower wavevector transfer values for both positive and negative α values. For $0 < \alpha \leq 2.5$, a clear minimum of scattering at low q ($qD/2\pi < 0.2$), and for α close to $\alpha_0 = D/2\overline{R} = 1.7$, is observed, while an increase of intensity is found above this value. On the contrary, the signal increases steadily for small q values when $\alpha < 0$. Whatever the sign of α, the autocorrelation oscillations observed at $\alpha = 0$ are strongly damped (Fig. 9).

3.5.3. The partial and total interference functions. The interference functions can help in understanding the above described behavior. The node–node total interference function $S(q)$ is simply obtained by replacing the object form factor by 1.0 in equation (49). The centered characteristic function $P_R(q) = \Omega(q)\exp[iq\lambda(q)]$ of the size distribution allows us to write

$$S(q) = 1 + 2\frac{\Omega^2(\alpha q)}{\Omega(2\alpha q)}\frac{\psi(q)\cos[u(q) + \zeta_0(q)] - \psi^2(q)\cos[\zeta_0(q)]}{1 + \psi^2(q) - 2\psi(q)\cos[u(q)]}, \quad (59)$$

where

$$\psi(q) = \phi(q)\Omega(2\alpha q) \quad (60)$$

$$u(q) = q[D + 2\alpha\lambda(2\alpha q)] \quad (61)$$

$$\zeta_0(q) = 2\alpha q[\lambda(\alpha q) - \lambda(2\alpha q)]. \quad (62)$$

In the case of normally distributed objects, the result is

$$S(q) = 1 + \exp(\alpha^2 q^2\sigma_R^2)\left[\frac{1 - \psi^2(q)}{1 + \psi^2(q) - 2\psi(q)\cos(qD)} - 1\right], \quad (63)$$

where $\psi(q) = \phi(q)\exp(-2\alpha^2 q^2\sigma_R^2)$. $S(q)$ and the pair correlation function $g(x)$ obtained by back Fourier transform are displayed in Fig. 10 for various correlation parameters α. As expected from equation (46), $S(q)$ is even with α. The variation of the parameter α allows a continuous transition from a system of correlated objects with a clear peak in the $S(q)$ and $g(x)$ functions to uncorrelated aggregated particles with a nearly flat pair correlation function. The interference peak broadens and shifts continuously with α towards low q values before disappearing around $\alpha = 2.5$. Within this model, the first conclusion is that even the position of the first peak of $S(q)$ is not directly proportional to the inverse of the mean object separation D. Secondly, the maximum observed below $qD/2\pi = 1$ for $\alpha > 2.5$ in the total scattered intensity (see Figs. 8 and 9) is not, strictly speaking, a correlation peak. By using the decomposition of $I(q)$ along the partial interference functions [equation (10)], it can be shown that, for $\alpha > 2.5$, this peak is linked to the scattering from the largest isolated

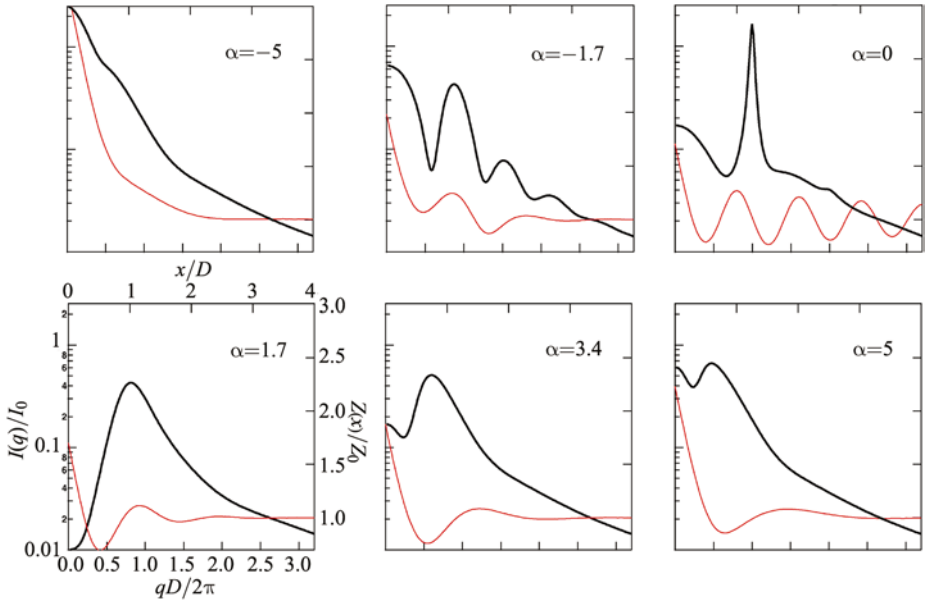

Figure 9
The total scattered intensity $I(q)/I_0$ (thick line) [equation (58)] and scattering-length autocorrelation function $z(x)/z_0$ (thin line) of a one-dimensional stick chain. The stick sizes are uncorrelated but the object separation depends linearly on the sizes of neighbors according to equation (46). The paracrystal statistic used is Gaussian [equation (22)] and the numerical parameters are those of equation (19).

objects. Another unusual result is the appearance of several maxima in the scattering curve for $\alpha < 0$ (see Fig. 9, $\alpha = -1.7$) that do not correspond to integer values of $qD/2\pi$. However, as a general rule, scattering from the largest particles dominates the observed pattern; depending on the sign of the α parameter, this can explain the general trends observed in Fig. 8: (i) the shift of the $qD/2\pi = 1$ peak towards small q values for $\alpha > 0$ as the largest objects are farther apart (see Fig. 7) and (ii) the intense small-angle scattering for $\alpha < 0$ as the largest particles tend to aggregate (see Fig. 7). These conclusions highlight the difficulty in analyzing experimental data for aggregated systems of particles at small and intermediate wavevector transfer, that is to say close to and below the 'correlation peak' $q \simeq 2\pi/D$. The partial interference functions can also be exactly evaluated:

$$S_{\ell m}(q) = 1 + 2\phi(q)\frac{\cos[\zeta_1(q)] - \psi(q)\cos[u(q) - \zeta_1(q)]}{1 + \psi^2(q) - 2\psi(q)\cos[u(q)]} \quad (64)$$

with $\zeta_1(q) = qD + \alpha(\Delta R_\ell + \Delta R_m)$ and $\psi(q)$ given by equation (62). As expected, the peak positions of the partial pair correlation functions $g_{\ell m}(x)$, obtained by Fourier transform of equation (64) (Fig. 11), follow obviously the $D + \alpha(\Delta R_\ell + \Delta R_m)$ rule. This distribution of preferential distances explains the non-Gaussian shape of the reflections in $g(x)$ and the disappearance of the 'correlation peak' above $\alpha \simeq 2.5$ (Fig. 10).

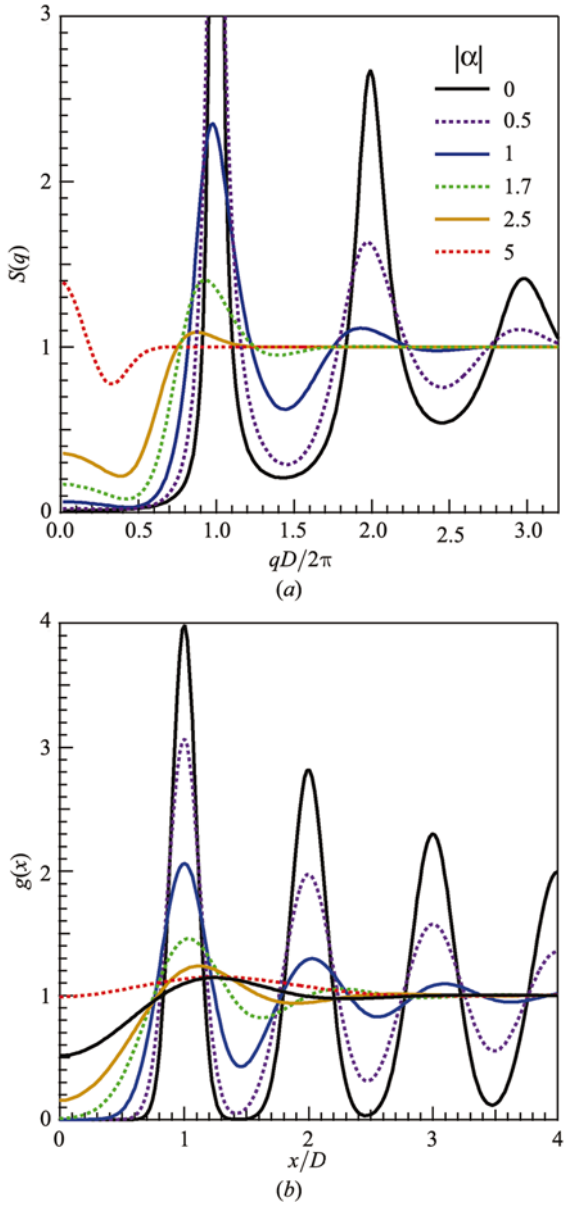

Figure 10
(*a*) The total interference function $S(q)$ [equation (63)] and (*b*) pair correlation function $g(x)$, calculated within the model of size–separation-distance correlation for various α values. The numerical parameters are those of equation (19).

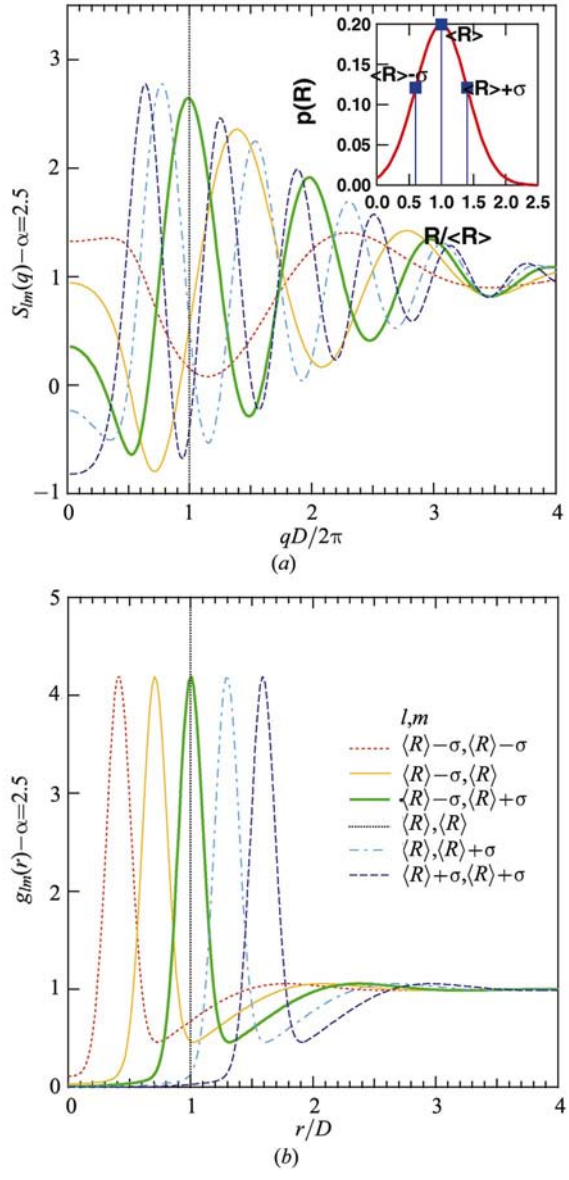

Figure 11
Examples of (*a*) partial interference functions, $S_{\ell m}(q)$, and (*b*) partial pair correlation functions $g_{\ell m}(x)$ evaluated in the framework of the size–separation-distance coupling model at $\alpha = 2.5$ with the parameters of equation (19). The points used in the size distribution $\ell, m = \overline{R} - \sigma, \overline{R}, \overline{R} + \sigma$ are shown in the inset.

3.5.4. The small wavevector transfer range. For either the stick case or the Dirac peak function, the $q = 0$ limit of the scattered intensity is given by

$$\lim_{q\to 0}\frac{I(q)}{\rho_0^2} = 4\overline{R}^2\frac{\sigma_D^2}{D^2} + 4\sigma_R^2\left(1 - 2\alpha\frac{\overline{R}}{D}\right)^2. \qquad (65)$$

The fluctuations of the scattering length in a probed volume (Guinier & Fournet, 1955; Guinier, 1963; Ziman, 1979) are reduced to those of the paracrystal alone when $\alpha = \alpha_0 = D/2\overline{R}$. This value corresponds to the small scattering-vector area of Fig. 8, where the scattered intensity is minimum. As already mentioned, this case leads to a scale invariant behavior; local changes in the density are expected to be drastically reduced at any site of the chain. This minimum of intensity due to size–distance correlation in the low-q range can explain, from our point of view, many results obtained by angle scattering on particle systems (Naudon *et al.*, 2000; Revenant *et al.*, 2004) as well as the inadequacy of LMA and DA when applied to data analysis. DA yields a too intense small-angle scattering (see Fig. 1) while LMA, which relies on an unphysical interpretation of the particle system, mimics the observed intensity minimum through an adequate interference function. It is tempting to characterize the aggregation process (see Fig. 7) that is observed in the size–distance correlation model by a Guinier gyration radius R_g as $\lim_{q\to 0} I(q) = I(q=0)(1 - q^2R_g^2/2)$. Fig. 12 displays R_g *versus* α for a stick shape; when R_g^2 is not defined, R_g is set to a negative value. The small-q expansion shows that R_g diverges with α and tends towards the limit value of $R_g^{lim} = 2\times 2^{1/2}\alpha^2\sigma_R^2/D^2$ at high α values; this limit $R_g^{\rm lim}$ does not depend on the mean size of the particle and varies with the particle density and the coupling parameter α. Thus for $|\alpha| > \alpha_0$, the aggregation of particles [see Fig. 7 ($\alpha = 5$)] drives the value of the observed gyration radius, which is far from that of purely isolated objects obtained from equation (16):

$$R_g^s = \left(\frac{\overline{R}^4/3 + 2\sigma_R^2\overline{R}^2 + \sigma_R^4}{\overline{R}^2 + \sigma_R^2}\right)^{1/2}. \qquad (66)$$

Thus, even though a correlation peak seems to be absent in the scattering curve, the Guinier gyration radius analysis is not necessarily valid.

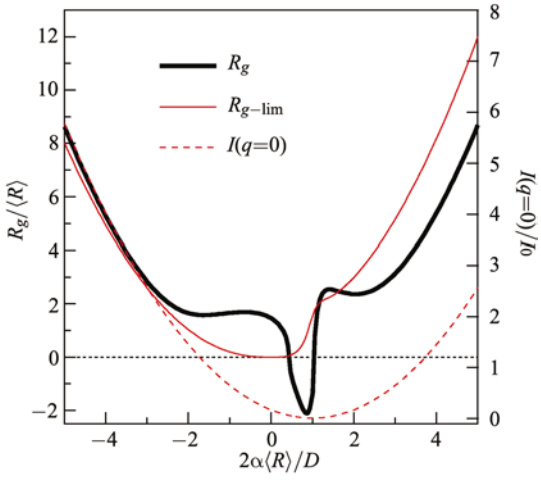

Figure 12
The gyration radius R_g within the aggregation model. R_g is normalized by the mean radius $\overline{R}$ and plotted *versus* the normalized correlation coefficient $\alpha/\alpha_0 = 2\alpha\overline{R}/D$. Also displayed are the $q = 0$ scattering intensity and the high-α limit of the gyration radius. The numerical parameters are given in equation (19).

3.6. Correlations between sizes and the fluctuations of separation distance: cumulative size and relative position disorder

3.6.1. Approach for a Gaussian paracrystal. The last correlation type that is taken into account is the coupling between the sizes of the objects and the disorder of the internode distances. If we neglect any size–size or size–separation distance coupling, the simplest analytical form is to add to the distance variance a term that depends linearly on the size of the nearest neighbors:

$$\int_{-\infty}^{+\infty} d_n^2\mathcal{P}(d_n/[R_0,\ldots,R_n])\,{\rm d}d_n - \left[\int_{-\infty}^{+\infty} d_n\mathcal{P}(d_n/[R_0,\ldots,R_n])\,{\rm d}d_n\right]^2 = \sigma_D^2 + \beta^2(\Delta R_{n-1} + \Delta R_n)^2. \qquad (67)$$

From this expression, it appears that increasing the coupling parameter β or the size distribution will degrade the long-range order of the paracrystal. A sketch of the chain is displayed in Fig. 13. To obtain tractable results, the paracrystal internode spacing is restricted to the Gaussian case. If one keeps in mind that the first moments of a probability law are given by the first terms of the small-q expansion of its characteristic function, this Gaussian hypothesis leads to results identical to any type of probability law at least up to second order in q. This hypothesis yields

$$P(q/[R_0,\ldots,R_n]) = \exp(-iqD)\exp\left\{-\frac{q^2}{2}[\sigma_D^2 + \beta^2(\Delta R_{n-1} + \Delta R_n)^2]\right\}. \qquad (68)$$

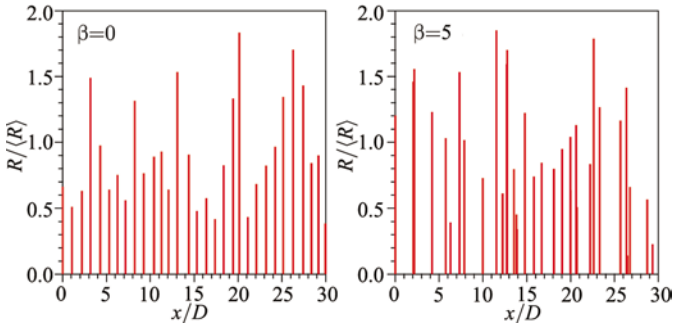

Figure 13
A sketch of a stick chain with Gaussian disorders (size $\sigma_R = 0.4\overline{R}$ and separation distance $\sigma_D = 0.1D$) with a coupling parameter β between the neighbor sizes and the variance of distance between objects [equation (67)].

Equation (7) gives the total scattering intensity with this model of disorder:

$$I(q) = \langle |F(q,R)|^2 \rangle + \sum_{n=1}^{+\infty} I_c^n(q)\cos(nqD) \tag{69}$$

$$I_c^n(q) = \int\!\!\ldots\!\!\int p(R_0)\ldots p(R_n)F^*(q,R_0)F(q,R_n) \times \prod_{k=1}^{n}\exp\left\{-\frac{q^2}{2}[\sigma_D^2+\beta^2(\Delta R_{k-1}+\Delta R_k)^2]\right\} \mathrm{d}R_0\ldots\mathrm{d}R_n.$$

With a Gaussian size distribution [equation (14)], the multiple integral in the previous equation is replaced by

$$I_c^n(q) = \frac{\exp[-n(q^2\sigma_D^2/2)]}{[\sigma_R(2\pi)^{1/2}]^{n+1}}\int\!\!\ldots\!\!\int \exp\left[-\frac{1}{2\sigma_R^2}\mathcal{S}(\Delta R_0,\ldots,\Delta R_n)\right] \times F(q,R_0)F(q,R_n)\,\mathrm{d}R_0\ldots\mathrm{d}R_n, \tag{70}$$

where $\mathcal{S}(\Delta R_0,\ldots,\Delta R_n)]$ is a positive definite quadratic form:

$$\mathcal{S}(\Delta R_0,\ldots,\Delta R_n) = (1+\kappa)(\Delta R_0^2+\Delta R_n^2)+(1+2\kappa)\sum_{k=1}^{n-1}\Delta R_k^2 + 2\kappa\sum_{k=1}^{n}\Delta R_{k-1}\Delta R_k, \tag{71}$$

with $\kappa = \beta^2 q^2\sigma_R^2$. In order to compute $I_c^n(q)$, one needs (i) to diagonalize the quadratic form of equation (71) and (ii) to express the form factors in the basis of eigenvectors X_k of $\mathcal{S}(\Delta R_0,\ldots,\Delta R_n)$. The method is described in Appendix *B* and only the final results are given here.

3.6.2. Specific object shapes.

The Dirac peak object

The total scattered intensity (see Appendix *B*.1) involves the determinant γ_n [equation (73)] of the matrix $\mathbf{A}_{\mathcal{S}}$ associated with the quadratic form [equation (71)]:

$$I(q) = 4\rho_0^2(\overline{R}^2+\sigma_R^2)+8\rho_0^2\sum_{n=1}^{+\infty}\frac{1}{(\gamma_n)^{1/2}}[\overline{R}^2+\sigma_R^2\zeta_n] \times \exp\left[-n\frac{q^2\sigma_D^2}{2}\right]\cos(nqD) \tag{72}$$

with

$$\begin{aligned}\zeta_n &= (-1)^n\kappa^n/\gamma_n\\ \gamma_n &= (1+2\kappa)\gamma_{n-1}-\kappa^2\gamma_{n-2}\\ \gamma_1 &= 1+2\kappa,\quad \gamma_2 = (1+\kappa)(1+3\kappa).\end{aligned} \tag{73}$$

The stick object

The stick-case calculation (Appendix *B*.2) leads to the scattering expression

$$I(q) = \frac{2\rho_0^2}{q^2}[1-\exp(-2\sigma_R^2q^2)\cos(2q\overline{R})]+\frac{8\rho_0^2}{q^2}\sum_{n=1}^{+\infty}\frac{1}{(\gamma_n)^{1/2}} \times\{\sinh(q^2\sigma_R^2\zeta_n)\cos^2(q\overline{R})+\cosh(q^2\sigma_R^2\zeta_n)\sin^2(q\overline{R})\} \times\exp[-q^2\sigma_R^2\mu_n]\exp\left[-n\frac{q^2\sigma_D^2}{2}\right]\cos(nqD) \tag{74}$$

with

$$\mu_1 = \frac{1+\kappa}{1+2\kappa},\quad \mu_2 = \frac{1+3\kappa+\kappa^2}{1+3\kappa},\quad \mu_n = (1+\kappa)\left(1-\kappa\frac{\gamma_{n-1}}{\gamma_n}\right). \tag{75}$$

The main consequence (Fig. 14) of an increasing coupling between the sizes of the scattering entities and the variance of their distance disorder is an increase of diffuse scattering close to the origin and a slight shift and a broadening of the correlation peak.

3.6.3. The total interference function. By using the basis change [equation (82)], the node–node interference function $S(q)$ is obtained straightforwardly from equation (69) by suppressing the form-factor expressions:

$$S(q) = 1+2\sum_{n=1}^{+\infty}\frac{1}{(\gamma_n)^{1/2}}\exp\left[-n\frac{q^2\sigma_D^2}{2}\right]\cos(nqD). \tag{76}$$

As shown in Fig. 15, increasing the coupling parameter β degrades the long-range order, but without any noticeable shift of the interference function peaks contrary to the behavior of the 'correlation peak' in Fig. 14.

4. Conclusions and model generalization

An extension of the one-dimensional paracrystal model has been developed to mix the well known substitution and lattice disorders in the framework of the paracrystal, thus including correlations between the cell scattering weights and lattice sites. Based on a probabilistic description of the scattering-length autocorrelation function, the diffuse scattering as well as the total and partial interference functions were evaluated. Simple analytical expressions were given in the case of first-neighbor correlations between size, separation distance and variance of separation distance for simple objects in the form of sticks and Dirac peaks. In the size–size correlation case, the coupling parameter ρ allows for a continuous transition from the decoupling approximation (analogous to the static Debye–Waller approximation) to the local monodisperse approximation (incoherent interference between monodisperse domains). The correlation to the nth neighbor is found to decrease as $|\rho|^n$. The case $\rho<0$ corresponds to an alternation of neighboring particles that are very dissimilar in size, leading in the limit case $\rho=-1$ to a pseudo-doubling of the unit cell and hence a doubling of the number of Bragg peaks. With increasing $|\rho|$, the intensity increases below Bragg peaks with a corresponding decrease of the diffuse scattering in between, thus illustrating the somewhat arbitrary distinction between coherent and diffuse scattering. The second model introduces a link between the object scattering length and their separation, the most obvious being a hard-core repulsion. In this case, peculiar features have been highlighted as (i) the ability to find a peak in the total scattered curve without any structure in the total interference function, (ii) a specific value of the coupling parameter which leads to a scale invariant behavior and reduces the total scattered intensity at $q=0$ and (iii) a

continuous shift of the first peak of intensity towards low wavevector transfer with increasing coupling parameter, whose position is no longer simply related to the averaged nearest-neighbor separation D. In addition, large size–separation coupling may even yield a peak in intensity that can no longer be interpreted as a 'correlation peak' since it is dominated by the largest particles. These findings show the difficulty of interpreting experimental data for correlated particles at small and intermediate wavevector transfers, close to the first peak of intensity. In the last model of correlation, with increasing coupling, an increase of diffuse scattering and a smoothing of the correlation peak is observed. A mixture of coupling or other probability laws can also be foreseen, the chosen examples herein giving only an illustration of the general method. The practical application of such a formal treatment to the experimental problem of X-ray small-angle scattering from particles and its straightforward extension to diffraction from a random stacking of layers or from terraces on surfaces will be the topics of a forthcoming paper.

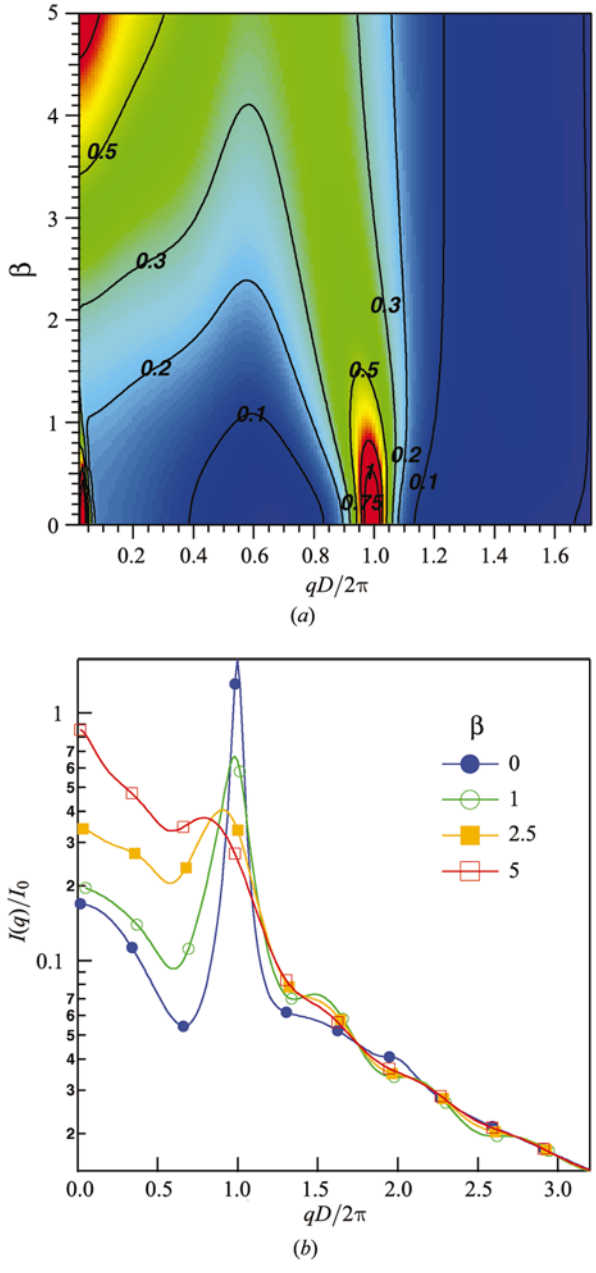

Figure 14
(*a*) A map in the (q, β) space of the diffuse scattering from a paracrystalline stick chain, whose separation-distance disorder variance is correlated to the particle sizes. (*b*) Intensity cuts for various β parameters. The intensity normalized by $I_0 = 4\rho_0^2\overline{R}^2$ is calculated from the parameters of equation (19).

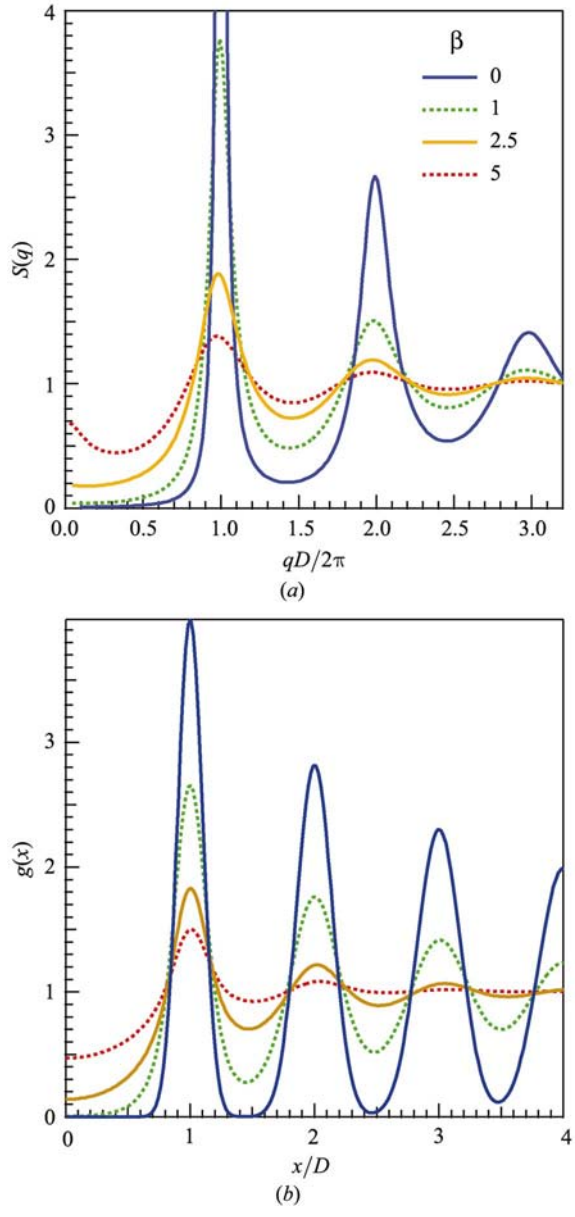

Figure 15
(*a*) Total interference function $S(q)$ and (*b*) node–node pair correlation function $g(x)$ for a one-dimensional Gaussian paracrystal with size–separation-distance disorder coupling. The coupling parameter β is defined in equation (67). The numerical parameters are given in equation (19).

APPENDIX *A*
Useful geometric sums

The four following sums often come into play in the discussed models; they are calculated using the geometric series sum:

$$2\sum_{n=1}^{+\infty}\phi^n\cos(nu) = \frac{1}{1-\phi\exp(iu)} + \frac{1}{1-\phi\exp(-iu)} - 2$$
$$= 2\phi\frac{\cos(u)-\phi}{1+\phi^2-2\phi\cos(u)}$$
$$= \frac{1-\phi^2}{1+\phi^2-2\phi\cos(u)} - 1 \qquad (77)$$

$$2\sum_{n=0}^{+\infty}\phi^{2n+1}\cos[(2n+1)u] = \frac{\phi\exp(iu)}{1-\phi^2\exp(i2u)} + \frac{\phi\exp(-iu)}{1-\phi^2\exp(-2iu)}$$
$$= 2\phi\cos(u)\frac{1-\phi^2}{1+\phi^4-2\phi^2\cos(2u)} \qquad (78)$$

$$2\sum_{n=1}^{+\infty}\phi^{2n}\cos[2nu] = \frac{1}{1-\phi^2\exp(i2u)} + \frac{1}{1-\phi^2\exp(-2iu)} - 2$$
$$= 2\phi^2\frac{\cos(2u)-\phi^2}{1+\phi^4-2\phi^2\cos(2u)} \qquad (79)$$

$$2\sum_{n=1}^{+\infty}\phi^n\sin(nu) = \frac{1}{i}\left(\frac{1}{1-\phi\exp(iu)} - \frac{1}{1-\phi\exp(-iu)}\right)$$
$$= \frac{2\phi\sin(u)}{1+\phi^2-2\phi\cos(u)}. \qquad (80)$$

Obviously, $|\phi| < 1$ as it is always the Fourier transform of a probability law.

APPENDIX *B*
Size–separation-distance disorder coupling: how to compute the $I_c^n(q)$ integrals

In the basis of ΔR_k, the matrix $\mathbf{A}_{\mathcal{S}}$ of size $n+1$, associated with the quadratic form $\mathcal{S}(\Delta R_0, \ldots, \Delta R_n)$ [equation (71)], is the following tridiagonal matrix:

$$\mathbf{A}_{\mathcal{S}} = \begin{pmatrix} 1+\kappa & \kappa & 0 & \ldots & & & \\ \kappa & 1+2\kappa & \kappa & 0 & \ldots & & \\ 0 & \kappa & 1+2\kappa & \kappa & 0 & \ldots & \\ \vdots & \ddots & \ddots & \ddots & \ddots & \ddots & \vdots \\ & \ldots & 0 & \kappa & 1+2\kappa & \kappa & 0 \\ & & \ldots & 0 & \kappa & 1+2\kappa & \kappa \\ & & & \ldots & 0 & \kappa & 1+\kappa \end{pmatrix} \qquad (81)$$

with $\kappa = \beta^2 q^2 \sigma_R^2$. As $\mathbf{A}_{\mathcal{S}}$ is symmetric and real, there is a change of basis that diagonalizes it. Let us call (i) X_k this basis and (ii) $\mathbf{P}$ the basis change matrix from X_k to ΔR_k according to

$$\Delta R_k = \sum_{i=0}^{n} P_{ki} X_i, \qquad (82)$$

and call $\mathbf{D}_{\mathcal{S}}$ the diagonal form of $\mathbf{A}_{\mathcal{S}}$ in the X_k basis. Thus, $\mathbf{A}_{\mathcal{S}} = \mathbf{P}\mathbf{D}_{\mathcal{S}}\mathbf{P}^{-1}$ with $\mathbf{P}^{-1} = {}^t\mathbf{P}$ (${}^t\mathbf{P}$ being the transposed matrix of $\mathbf{P}$). In the X_k basis, the quadratic form takes the following simple expression:

$$\mathcal{S}(X_0, \ldots, X_n) = \sum_{k=0}^{n} D_{kk} X_k^2. \qquad (83)$$

As $\mathbf{P}$ is an orthogonal basis change, its determinant is equal to one; thus the variable change from ΔR_k to X_k in the integral of equation (70) results in a Jacobian equal to one. The remaining task, in order to compute the multiple integral of equation (70), is to express the form factor in equations (12)–(13) in the X_k basis by using equation (82). In the following, the determinant γ_n of the matrix $\mathbf{A}_{\mathcal{S}}$ will be used. It can be evaluated recursively through an expansion along one column:

$$\det\mathbf{A}_{\mathcal{S}} = \gamma_n = (1+2\kappa)\gamma_{n-1} - \kappa^2\gamma_{n-2}$$
$$\text{with} \quad \gamma_1 = 1+2\kappa, \quad \gamma_2 = (1+\kappa)(1+3\kappa). \qquad (84)$$

B1. The Dirac peak object

By using the form-factor expression in equation (12) and the variable change X_k [equations (82), (83)], equation (70) takes the following form:

$$I_c^n(q) = 8\rho_0^2\frac{\exp[-nq^2(\sigma_D^2/2)]}{[\sigma_R(2\pi)^{1/2}]^{n+1}}\int\ldots\int\exp\left[-\frac{1}{2\sigma_R^2}\sum_{k=0}^{n}D_{kk}X_k^2\right]$$
$$\times\left(\overline{R}+\sum_{k=0}^{n}P_{0k}X_k\right)\left(\overline{R}+\sum_{k=0}^{n}P_{nk}X_k\right)\mathrm{d}X_0\ldots\mathrm{d}X_n. \qquad (85)$$

The integration over a normally distributed variable is easily handled:

$$I_c^n(q) = 8\rho_0^2\exp\left[-n\frac{q^2\sigma_D^2}{2}\right]\prod_{k=1}^{n}\frac{1}{(D_{kk})^{1/2}}\left[\overline{R}^2+\sigma_R^2\sum_{k=0}^{n}\frac{P_{0k}P_{nk}}{D_{kk}}\right]. \qquad (86)$$

Using the properties of the determinant, notice that

$$\prod_{k=1}^{n}\frac{1}{(D_{kk})^{1/2}} = \frac{1}{(\gamma_n)^{1/2}}. \qquad (87)$$

Also, as $\mathbf{P}^{-1} = {}^t\mathbf{P}$, one finds

$$\sum_{k=0}^{n}\frac{P_{0k}P_{nk}}{D_{kk}} = \sum_{k=0}^{n}P_{0k}D_{kk}^{-1}P_{kn}^{-1} = [\mathbf{P}\mathbf{D}\mathbf{P}^{-1}]_{0n} = [\mathbf{A}_{\mathcal{S}}^{-1}]_{0n}. \qquad (88)$$

This term can be computed directly from the matrix expression (81) of $\mathbf{A}_{\mathcal{S}}$:

$$[\mathbf{A}_{\mathcal{S}}^{-1}]_{0n} = (-1)^n\frac{\kappa^n}{\gamma_n} = \zeta_n. \qquad (89)$$

By gathering equations (86)–(89) in equation (69) together with equation (15), the total intensity scattered [equation (72)] by a Dirac peak particle with a size–separation-distance disorder coupling is found.

B2. The stick object

The stick case is handled in the same way as in the previous calculation:

$$I_c^n(q) = \frac{8\rho_0^2}{q^2}\frac{\exp[-n(q^2\sigma_D^2/2)]}{[\sigma_R(2\pi)^{1/2}]^{n+1}}\int\cdots\int \exp\left[-\frac{1}{2\sigma_R^2}\sum_{k=0}^{n} D_{kk}X_k^2\right] \times \sin\left(\overline{R}+\sum_{k=0}^{n} P_{0k}X_k\right)\sin\left(\overline{R}+\sum_{k=0}^{n} P_{nk}X_k\right)\mathrm{d}X_0\ldots\mathrm{d}X_n. \quad (90)$$

The transformation in a complex number of the sine which appears in the form-factor expression yields

$$I_c^n(q) = -\frac{2\rho_0^2}{q^2}\frac{\exp[-n(q^2\sigma_D^2/2)]}{[\sigma_R(2\pi)^{1/2}]^{n+1}}\int\cdots\int \exp\left[-\frac{1}{2\sigma_R^2}\sum_{k=0}^{n} D_{kk}X_k^2\right] \times \left\{\exp\left[iq\left(2\overline{R}+\sum_{k=0}^{n}(P_{0k}+P_{nk})\right)\right] - \exp\left[iq\sum_{k=0}^{n}(P_{0k}-P_{nk})+\text{c.c.}\right]\right\}\mathrm{d}X_0\ldots\mathrm{d}X_n. \quad (91)$$

Using the Fourier transform of a Gaussian, the previous equation reads

$$I_c^n(q) = \frac{4\rho_0^2}{q^2}\exp\left[-n\frac{q^2\sigma_D^2}{2}\right]\left\{\prod_{k=0}^{n}\frac{1}{(D_{kk})^{1/2}} \times \exp\left[-\frac{q^2\sigma_R^2}{2}\left(\frac{P_{0k}^2+P_{nk}^2}{D_{kk}}\right)\right]\right\}\left\{\prod_{k=0}^{n}\exp\left[\frac{q^2\sigma_R^2P_{0k}P_{nk}}{D_{kk}}\right] - \cos(2q\overline{R})\prod_{k=0}^{n}\exp\left[-\frac{q^2\sigma_R^2P_{0k}P_{nk}}{D_{kk}}\right]\right\}. \quad (92)$$

It appears that

$$\prod_{k=0}^{n}\exp\left[\pm q^2\sigma_R^2\frac{P_{0k}P_{nk}}{D_{kk}}\right] = \exp\left[\pm q^2\sigma_R^2\sum_{k=0}^{n}\frac{P_{0k}P_{nk}}{D_{kk}}\right] = \exp(\pm q^2\sigma_R^2[\mathbf{A}_{\mathcal{S}}^{-1}]_{0n}), \quad (93)$$

$$\prod_{k=0}^{n}\exp\left[-\frac{q^2\sigma_R^2}{2}\frac{P_{0k}^2+P_{nk}^2}{D_{kk}}\right] = \exp\left[-\frac{q^2\sigma_R^2}{2}([\mathbf{A}_{\mathcal{S}}^{-1}]_{00}+[\mathbf{A}_{\mathcal{S}}^{-1}]_{nn})\right]. \quad (94)$$

The term $[\mathbf{A}_{\mathcal{S}}^{-1}]_{0n}$ has already been calculated in equation (89). The two others can be computed recursively using the expression of the associated matrix cofactors which involves the global matrix determinant:

$$[\mathbf{A}_{\mathcal{S}}^{-1}]_{00} = [\mathbf{A}_{\mathcal{S}}^{-1}]_{nn} = \frac{1}{\gamma_n}(1+\kappa)(\gamma_n-\kappa\gamma_{n-1}). \quad (95)$$

Finally, by gathering in equation (69) the results found in equations (92)–(95), the scattered intensity expressed in equation (74) is obtained.

References

Busson, B. & Doucet, J. (2000). *Acta Cryst.* A**56**, 68–72.
Croset, B. & de Beauvais, C. (1997). *Surf. Sci.* **384**, 15–35.
Croset, B. & de Beauvais, C. (1998). *Surf. Sci.* **409**, 403–412.
Eads, J. & Millane, R. (2000). *Acta Cryst.* A**56**, 549–553.
Eads, J. & Millane, R. (2001). *Acta Cryst.* A**57**, 507–517.
Guinier, A. (1956). *Théorie et Technique de la Radiocristallographie.* Paris: Dunod.
Guinier, A. (1963). *X-ray Diffraction in Crystals, Imperfect Crystals and Amorphous Bodies.* New York: Dover Publications.
Guinier, A. & Fournet, G. (1955). *Small-Angle Scattering of X-rays.* New York: John Wiley and Sons.
Hosemann, R. (1951). *Acta Cryst.* **4**, 520–530.
Hosemann, R. & Bagchi, S. N. (1962). *Direct Analysis of Diffraction by Matter.* Amsterdam: North-Holland.
Hosemann, R. & Hindeleh, A. (1995). *J. Macromol. Sci. Phys.* B**34**, 327–356.
Lazzari, R. (2002). *J. Appl. Cryst.* **35**, 406–421.
Matsuoka, H., Tanaka, H., Hashimoto, T. & Ise, N. (1987). *Phys. Rev. B*, **36**, 1754–1765.
Matsuoka, H., Tanaka, H., Hashimoto, T. & Ise, N. (1990). *Phys. Rev. B*, **41**, 3854–3856.
Metzger, T. H., Kegel, I., Paniago, R., Lorke, A., Peisl, J., Schulze, J., Eisele, I., Schittenhelm, P. & Abstreiter, G. (1998). *Thin Solid Films*, **336**(8), 1–8.
Millane, R. & Eads, J. (2000). *Acta Cryst.* A**56**, 497–506.
Mu, X.-Q. (1998). *Acta Cryst.* A**54**, 606–616.
Naudon, A., Babonneau, D., Thiaudière, D. & Lequien, S. (2000). *Physica (Utrecht)*, B**283**, 69–74.
Pedersen, J. (1997). *Adv. Colloid Interface Sci.* **70**, 171–210.
Pedersen, J. S. (1994). *J. Appl. Cryst.* **27**, 595–608.
Pedersen, J. S., Vysckocil, P., Schönfeld, B. & Kostorz, G. (1997). *J. Appl. Cryst.* **30**, 975–985.
Renaud, G., Lazzari, R., Revenant, C., Barbier, A., Noblet, M., Ulrich, O., Leroy, F., Jupille, J., Borenstzein, Y., Henry, C. R., Deville, J. P., Scheurer, F., Mane-Mane, J. & Fruchart, O. (2003). *Science*, **300**, 1416–1419.
Revenant, C., Leroy, F., Lazzari, R., Renaud, G. & Henry, C. (2004). *Phys. Rev. B*, **69**, 035411–1.
Stroud, W. & Millane, R. (1996). *Proc. R. Soc. London Ser. A*, **452**, 151–173.
Vignaud, G., Gibaud, A., Wang, J., Sinha, S., Daillant, J., Grüber, G. & Gallot, Y. (1997). *J. Phys. Condens. Matter*, **9**, L125–L130.
Warren, B. E. (1969). *X-ray Diffraction.* New York: Dover Publications.
Waseda, Y. (1980). *The Structure of Non-crystalline Materials.* New York: McGraw-Hill.
Welberry, T. (1985). *Rep. Prog. Phys.* **48**, 1543.
Welberry, T., Miller, G. & Carroll, C. (1980). *Acta Cryst.* A**36**, 921–929.
Ziman, J. M. (1979). *Models of Disorder.* Cambridge University Press.